Compatible microstructures in magnetic materials

Ananya Renuka Balakrishna *

Aerospace and Mechanical Engineering, University of Southern California, Los Angeles, California 90089, USA

(Received 9 December 2021; accepted 2 June 2022; published 13 July 2022)

A mathematical relationship between magnetic material constants is proposed for which highly reversible microstructures form during phase transformations. The microstructures formed during paramagnetic-to-ferromagnetic phase transformation are systematically studied, and specific combinations of material constants—namely, magnetocrystalline anisotropy κ_1, κ_2 and magnetostriction $\lambda_{100}, \lambda_{111}$—for which stress-free interfaces with divergence-free magnetization can form are identified. The microstructural analysis shows that magnetic materials with $\kappa_1 \leqslant 0, \kappa_2 \geqslant \frac{9|\kappa_1|}{4}$, and $\lambda_{111} = -\frac{\lambda_{100}}{3}$ form exactly compatible and divergence-free phase boundaries. Furthermore, the analysis shows that, consistent with experimental observation, magnetic alloys that undergo cubic-to-monoclinic-II transformation have multiple solutions satisfying the high-reversibility condition and are suitable candidates for alloy development. Broadly, the results could guide the design of magnetic materials with low fatigue and hysteresis for energy applications.

DOI: 10.1103/PhysRevMaterials.6.074402

I. INTRODUCTION

Magnetic materials that undergo diffusionless phase transformations are characterized by an abrupt change in physical properties (e.g., paramagnetic to ferromagnetic). This abrupt change makes phase transformation magnetic materials most exciting in science and technology, and in recent years, their use in rewritable optical memories, magnetic refrigeration, and induction motors of electric vehicles has seen enormous growth [1,2]. Although magnetic materials are commonly used, their widespread application is limited by the decay of material properties with repeated cycling [3]. In this paper, we systematically study the microstructures that form in magnets during phase transformations and propose a mathematical relationship between magnetic material constants that can be used to significantly reduce (or eliminate) material decay.

A leading cause of decay of material properties during phase transformation is attributed to the elastically stressed phase boundary that separates the ferromagnetic and paramagnetic phases [4,5]. During phase transformation, individual lattices undergo abrupt structural changes that induce significant stresses at the phase boundary. This stressed phase boundary, which moves back and forth in the material during phase transformation, can nucleate defects, anisotropically expand materials, and contribute to the irreversible decay of magnetic properties. Additionally, this phase boundary serves as a nucleation barrier during reversible cycling and induces thermal hysteresis [4]. Consequently, these phase transformation magnetic materials need to be replaced after a few hundred cycles. Under ideal circumstances, many applications using these magnetic materials need to be *reversibly* cycled at high frequencies, and for over several thousand times in a single lifespan.

Shape-memory alloys—another class of phase transformation materials—bear similarities to magnetic materials and undergo structural degradation with repeated cycling. However, researchers have recently discovered crystallographic design principles according to which shape-memory alloys with small hysteresis and high reversibility can be atomically engineered. For example, a Ti-Ni-Cu alloy that typically fatigues after 200 stress-strain cycles was atomically doped to satisfy a $\lambda_2 = 1$ design condition [6]. This design condition corresponds to a special set of lattice parameters for which a phase transformation material can form a stress-free interface between the two phases [7]. By satisfying this design condition the shape-memory alloy forms an exactly compatible and stress-free phase boundary that dramatically lowers its hysteresis [8]. In another example, a highly reversible shape-memory alloy was atomically doped to satisfy the cofactor conditions [9]. These doped alloys not only form stress-free phase boundaries, but also have an infinite number of solutions for which the stress-free phase boundaries can form. These infinite solutions offer extraordinary reversibility to shape-memory alloys. These crystallographic design principles are being used to design novel shape-memory alloys and have been adapted to other phase transformation materials, including semiconductors, ferroelectrics, ferromagnets, and intercalation materials [10–16].

However, unlike shape-memory alloys, phase transformations in magnetic materials are accompanied by an abrupt change in the magnetization state in addition to the structural transformation of its lattices. While the design principles, such as the $\lambda_2 = 1$ and the cofactor conditions, ensure structural compatibility at the phase boundary and minimize the elastic energy, we do not know whether these phase boundaries will have divergence-free magnetization that is necessary for minimum demagnetization energy [4,5,17]. Although magnetization compatibility follows structural compatibility for twin interfaces between magnetic variants [18], this is not a

*renukaba@usc.edu

necessary and sufficient condition for an exactly compatible paramagnetic/ferromagnetic interface. The demagnetization energy, if not minimized, would restrict the microstructural solutions for compatible interfaces and thus affect the reversible cycling of magnetic materials.

Another limitation in applying the crystallographic design principles to magnetic alloys is related to the fundamental coupling between lattice deformations and the magnetic material constants, such as magnetocrystalline-anisotropy constants κ_1, κ_2 and magnetostriction constants $\lambda_{100}, \lambda_{111}$. The values of the anisotropy constants κ_1, κ_2 determine the easy axes of magnetization (i.e., the crystallographic directions of magnetization) and thus affect lattice deformations [19]. Likewise, the magnetostriction constants $\lambda_{100}, \lambda_{111}$ determine how a material expands or contracts in response to its magnetization state and thus govern the lattice strains during phase transformations [20]. In materials with large magnetostriction (e.g., magnetic shape-memory alloys) these magnetostriction constants significantly contribute to the elastic energy of the system and play an important role in microstructural evolution. We do not know whether a specific combination of magnetic material constants—analogous to the $\lambda_2 = 1$ condition—exists for magnetic materials, for which structurally compatible and divergence-free microstructures can form during phase transformations. Such a condition would guide the design of magnetic alloys with high reversibility and low hysteresis [21].

The aim of the present work is to determine the combination of magnetic material constants for which compatible and divergence-free microstructures form in magnetic materials during phase transformation. We use the coupled strain tensor $\mathbf{E}_0$, which is a function of the magnetostriction constants $\lambda_{100}, \lambda_{111}$ and magnetization $\mathbf{m}$, in our microstructural analysis [22]. We apply the geometrically linear strain tensor $\mathbf{E}_0$ to determine the combination of magnetic material constants for which divergence-free twin interfaces, $\lambda_2 = 1$ paramagnetic/ferromagnetic interfaces, and cofactor microstructures form during phase transformation. Our microstructural analysis shows that magnetic alloys undergoing cubic-to-monoclinic-I transformation (with $\kappa_1 \leqslant 0$, $\kappa_2 \geqslant \frac{9|\kappa_1|}{4}$, and $\lambda_{111} = -\frac{\lambda_{100}}{3}$) form exactly compatible ($\lambda_2 = 1$) and divergence-free phase boundaries. Although other magnetic alloys, which undergo cubic-to-tetragonal or cubic-to-trigonal transformation, can form exactly compatible phase boundaries, these boundaries are not divergence-free. Additionally, our analysis shows that magnetic alloys that undergo cubic-to-monoclinic-II transformation have multiple solutions satisfying the exactly compatible and divergence-free conditions and are suitable for alloy development. Overall, our findings contribute to the design principles necessary to form highly reversible microstructures in magnetic alloys. In principle our microstructural analysis is transferable to other multiferroic materials, such as ferroelectrics; however, for the current study we use magnetic martensites as representative materials.

II. PHASE TRANSFORMATION IN MAGNETIC MATERIALS

Following Ball and James [26] and Song *et al.* [9], we propose a free-energy functional for magnetic materials that undergo first-order reversible phase transformations. We list all notations of symbols used in this text and their descriptions in the Appendix.

We assume a cubic crystal symmetry for lattices in the paramagnetic austenite phase. The macroscale material body has a reference configuration $\mathcal{E} \subset \mathbb{R}^3$ at the Curie temperature $\theta_0 = \text{const}$ and has an oblate ellipsoid (pancake-shaped) geometry oriented as shown in Fig. 1(c). On reducing the temperature to below the Curie temperature, the paramagnetic austenite lattices change their geometry and gain a spontaneous magnetization (i.e., the paramagnetic phase becomes a ferromagnetic phase). We describe this phase transformation using a geometrically linearized setting: Below, we discuss how this linearized framework enables us to derive a mathematical relationship between the materials' magnetostriction constants (linear coupling coefficients) that are necessary to form compatible microstructures. The geometrically linear theory simplifies various microstructure calculations and is strictly applicable to materials with small deformations.

In the geometrically linear theory, we describe an infinitesimal change in lattice geometry using a strain tensor $\mathbf{y} = \mathbf{E}\mathbf{x}$, $\mathbf{x} \in \mathcal{E}$. This strain tensor $\mathbf{E}$ is described as the symmetric part of the displacement gradient $\mathbf{E} = \frac{1}{2}(\mathbf{H} + \mathbf{H}^{\mathrm{T}})$ and is applicable to materials with uniformly small displacement gradients [27]. For these small deformations, the strain tensor is related to the stretch tensor as $\mathbf{U} = \mathbf{I} + \mathbf{E}$. Here, $\mathbf{I}$ is a 3×3 identity matrix. Further comments on the strain tensor for materials with small strain and rotations are given in the Appendix. The nondimensionalized magnetization in an orthonormal basis $\mathbf{m} = \mathbf{M}/m_s$ is parallel to the cubic axes, and m_s is the saturation magnetization of the magnetic material [28].

The paramagnetic-to-ferromagnetic phase transformation leads to a change in lattice geometry and magnetization state at the Curie temperature; we assume the existence of a free energy ϕ which depends on the magnetization $\mathbf{m}$, strain tensor $\mathbf{E}$, and temperature θ. We assume this free energy $\phi(\mathbf{m}, \mathbf{E}, \theta)$ (a) to be invariant with respect to infinitesimal changes of frame (or infinitesimal rotations $\mathbf{W}$), i.e., $\phi(\mathbf{m}, \mathbf{H} + \mathbf{W}, \theta) = \phi(\mathbf{m}, \mathbf{H}, \theta) = \psi(\mathbf{m}, \mathbf{E}, \theta)|_{\mathbf{E}=\frac{1}{2}(\mathbf{H}+\mathbf{H}^{\mathrm{T}})}$, and (b) to exhibit symmetries implied by an appropriate form of the Cauchy-Born rule combined with the Ericksen-Pitteri neighborhood [30,31].

The above construction of the free energy leads to an energy-well landscape of the following type:

$$\psi(\mathbf{m} = 0, \mathbf{E} = 0, \theta) \leqslant \psi(\mathbf{m}, \mathbf{E}, \theta), \quad \theta > \theta_0, \tag{1a}$$

$$\psi(0, 0, \theta) = \psi(\mathbf{m}_1, \mathbf{E}_1, \theta) = \cdots = \psi(\mathbf{m}_n, \mathbf{E}_n, \theta) \leqslant \psi(\mathbf{m}, \mathbf{E}, \theta), \quad \theta = \theta_0, \tag{1b}$$

$$\psi(\mathbf{m}_1, \mathbf{E}_1, \theta) = \cdots = \psi(\mathbf{m}_n, \mathbf{E}_n, \theta) \leqslant \psi(\mathbf{m}, \mathbf{E}, \theta), \quad \theta < \theta_0, \tag{1c}$$

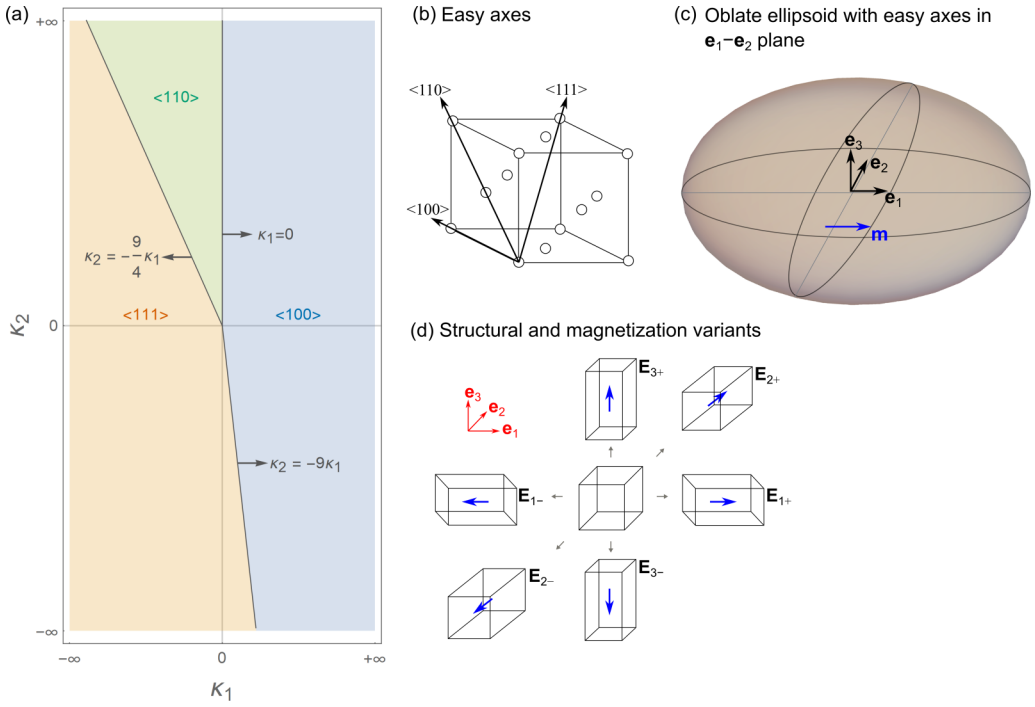

FIG. 1. (a) Easy axes of magnetization in soft magnets as a function of their anisotropy constants κ_1, κ_2 [19]. Three crystallographic directions, namely, $\langle 100\rangle$, $\langle 111\rangle$, and $\langle 110\rangle$, are found to be easy axes of magnetization in cubic alloys. (b) Schematic illustration of easy axes in a cubic unit cell. (c) In our calculations we assume the soft magnetic body to have a macroscale shape of an oblate ellipsoid with easy axes in plane. (d) Cubic-to-tetragonal transformation generates three structural variants $\mathbf{E}_1, \mathbf{E}_2, \mathbf{E}_3$ and six magnetization variants $\mathbf{E}_{1\pm}, \mathbf{E}_{2\pm}, \mathbf{E}_{3\pm}$.

where $\mathbf{E}_1 \cdots \mathbf{E}_n$ are the strain tensors that map an undistorted $\mathbf{E} = 0$ paramagnetic phase to the nth variant of the ferromagnetic phase. For temperatures above the Curie temperature $\theta > \theta_0$, a strain matrix near $\mathbf{E} = 0$ minimizes the free-energy function, and for temperatures below the Curie temperature $\theta < \theta_0$, strain matrices near $\mathbf{E}_1 \cdots \mathbf{E}_n$ minimize the free-energy function. In general the existence of $n+1$ energy wells for $\psi(\mathbf{m}, \mathbf{E}, \theta)$ leads to the formation of plate-like microstructures during phase transformations in magnetic materials. Each distinct well at $\mathbf{E} = 0, \mathbf{E}_1 \cdots \mathbf{E}_n$ is associated with a variant of the ferromagnetic phase, and the potential wells can be precisely derived from these lattice considerations [20]. Further details regarding the multiwell energy landscape are given in the Appendix. We note that a similar multiwell energy landscape with a suitable choice of order parameters and strain tensors can be used to describe paramagnetic-antiferromagnetic phase transformation in Pt-Mn alloys [32] and ferromagnetic-antiferromagnetic phase transformation in Mn-based alloys [33,34].

In this paper, we assume the bulk energy to be of the form in Eq. (1b) and derive microstructural solutions for compatible interfaces in magnetic alloys at the Curie temperature. Besides the bulk free-energy function, other energy terms such as the gradient energy and the demagnetization energy contribute to the total energy of the system:

$$\ominus = \int_{\mathcal{E}} \overbrace{\{\nabla \mathbf{m} \cdot A \nabla \mathbf{m}}^{\text{gradient energy}} + \overbrace{\psi(\mathbf{m}, \mathbf{E}, \theta)}^{\text{bulk energy}}\} d\mathbf{x} + \overbrace{\frac{\mu_0}{2} \int_{\mathbb{R}^3} |\nabla \zeta_{\mathbf{m}}|^2 d\mathbf{x}}^{\text{demagnetization energy}}. \tag{2}$$

The gradient energy penalizes gradients of the magnetization and is minimized when the neighboring magnetizations are parallel. The gradient energy constant is typically small (of the order of $A \approx 10^{-11}$ J/m^3), and we neglect its contribution at larger length scales. The demagnetization energy is related to the work required to arrange magnetic dipoles into a specific geometric configuration. This energy term scales quadratically with the demagnetization field $\mathbf{H}_{\mathrm{d}} = -\nabla \zeta_{\mathbf{m}}$, which is a gradient of the magnetostatic potential and is obtained by solving the magnetostatic equation, $\nabla \cdot (-\nabla \zeta_{\mathbf{m}} + \mathbf{M}) = 0$. The demagnetization energy is sensitive to the presence of defects in, and the body geometry of, the magnetic material. In our calculations we assume a perfectly smooth single-crystalline ellipsoid that (a) is free from defects and (b) forms magnetic microstructures that are pairwise compatible and thus locally divergence-free. This demagnetization energy can be minimized for a perfectly smooth ellipsoid with a constant average magnetization.

The ellipsoid geometry of the magnetic body is essential as a way of describing the magnetic poles on the boundary of an infinitely long macroscale body to minimize its demagnetization field. The demagnetization field $\mathbf{H}_{\mathrm{d}}$ is proportional to the magnetization intensity of the body and depends on the geometric shape of the body. For example, the demagnetization field is close to zero when the magnetic poles on the body are described to be far apart, such as at the two extreme ends of a rodlike body or on the farthest boundary edges of a disklike body. Furthermore, magnetic bodies with sharp edges or corners induce a nonzero demagnetization field, and in our calculations we assume a magnetic body with perfectly

smooth geometries such as an ellipsoid. This assumption of a general ellipsoid case of the magnetic material eliminates the effect of geometrical complications in deriving, as we do in Secs. III and IV, the balance of fundamental material constants that affect the formation of compatible microstructures. Furthermore, the ellipsoid configuration allows us to have magnetic microstructures with the strain $\mathbf{E}$ and magnetization $\mathbf{m}$ near the energy wells. Further details about treating the demagnetization field under external loads are derived in Ref. [18]. For our purposes, we use an oblate ellipsoid with easy magnetization axes of the material in plane and solve for compatible (and divergence-free) microstructures in the material bulk; see Fig. 1(c).

The bulk energy primarily accounts for two types of energy contributions. The first contribution is the anisotropy energy ψ_{aniso}, which is defined as the penalty paid for rotating the magnetization away from the direction of the easy crystallographic axes. This energy is a function of the magnetization vector $\mathbf{m}$ and material constants called the anisotropy constants κ_1, κ_2. For a cubic crystal the anisotropy energy ψ_{aniso} is expressed in ascending powers of the magnetization, and often the higher-order terms are neglected because of their small contributions:

$$\psi_{\text{aniso}} = \kappa_1\left(m_1^2m_2^2 + m_2^2m_3^2 + m_3^2m_1^2\right) + \kappa_2\left(m_1^2m_2^2m_3^2\right). \quad (3)$$

The constants κ_1, κ_2 measure the amount of anisotropy of a material, and their specific values determine the direction of easy crystallographic axes in a magnetic alloy. For example, in Fig. 1(a) the relation between κ_1 and κ_2 determines the easy axes of magnetization along three principal directions—$\langle 100\rangle$, $\langle 110\rangle$, and $\langle 111\rangle$—for a cubic crystal. The calculation of the easy axes is described in detail by Bozorth [19]. The three crystallographic easy axes of magnetization for cubic alloys are schematically illustrated in Fig. 1(b).

The second contribution (to the bulk energy) arises from the materials' magnetostrictive response. That is, when a body is magnetized (for example, under an externally applied magnetic field or during phase transformation), its dimensions change slightly. This relative change in a body's dimensions is referred to as magnetostriction and gives rise to the magnetoelastic energy of the system. The magnetoelastic energy is minimized for strains satisfying $\mathbf{E} = \mathbf{E}_0(\mathbf{m})$. Here, $\mathbf{E}_0(\mathbf{m})$ is the eigenstrain or the preferred strain tensor and is a function of magnetization orientation. In this paper, we use the general quadratic form of $\mathbf{E}_0(\mathbf{m})$ for a cubic case [20]:

$$\begin{aligned}\mathbf{E}_0(\mathbf{m}) &= \tfrac{3}{2}\Bigg(\lambda_{100}\left(\mathbf{m}\otimes\mathbf{m} - \tfrac{1}{3}\mathbf{I}\right) \\ &\quad + (\lambda_{111} - \lambda_{100})\sum_{i\neq j} m_i m_j(\mathbf{e}_i\otimes\mathbf{e}_j)\Bigg) \\ &= \tfrac{3}{2}\begin{bmatrix}\lambda_{100}\left(m_1^2 - \frac{1}{3}\right) & \lambda_{111}m_1m_2 & \lambda_{111}m_1m_3 \\ & \lambda_{100}\left(m_2^2 - \frac{1}{3}\right) & \lambda_{111}m_2m_3 \\ \text{symm.} & & \lambda_{100}\left(m_3^2 - \frac{1}{3}\right)\end{bmatrix},\end{aligned} \quad (4)$$

where "symm." refers to the matrix being symmetric.

Equation (4) describes lattice transformation using magnetostriction constants $\lambda_{100}, \lambda_{111}$ along two principal directions. Other constructions of strain matrices for magnetic materials with hexagonal symmetry (e.g., cobalt) would require more than two magnetostriction constants [19,35]. For our purposes, we assume a cubic (nonmagnetic) phase as the reference lattice and construct compatible microstructures during phase transformation. In Eq. (4) the magnetostriction constants $\lambda_{111}, \lambda_{100}$ and the magnetic dipole $\mathbf{m}$ determine the variants in the ferromagnetic phase of the material. We categorize these variants into two sets, namely, strain and magnetization variants. The strain variants ($\mathbf{E}_i$) describe the structural transformations of lattices, and the magnetization variants ($\mathbf{E}_{i\pm}$) describe the orientation of the magnetic dipole (e.g., $\pm\mathbf{m}$) in the transformed lattice; see Fig. 1(d). The direction of the magnetic dipole is governed by the anisotropy constants, and from Fig. 1(a) we identify the three crystallographic easy axes for magnetization to be $\langle 100\rangle$, $\langle 111\rangle$, and $\langle 110\rangle$, respectively. We assume saturation magnetization as input (i.e., $|\mathbf{m}| = 1$ or $|\mathbf{M}| = m_s$ as a constraint), and we compute the ferromagnetic strain and magnetization variants for each of the crystallographic easy axes; see the Appendix. We use the strain and magnetization variants to solve for compatible *and* divergence-free microstructures in magnetic alloys that can form during the paramagnetic-ferromagnetic phase transformation in Sec. III. Finally, we note that the form of the strain tensor in Eq. (4) can describe limited structural transformations (e.g., cubic to tetragonal, cubic to trigonal, and cubic to monoclinic-I) but other transformations such as cubic to orthorhombic or cubic to monoclinic-II that are widely observed in magnetic alloys [9,11,36–41] cannot be described using the general form of Eq. (4). We investigate this latter case in Sec. IV using a representative material.

III. COMPATIBLE INTERFACES

In this section, we determine for which combination of magnetostriction constants compatible interfaces with divergence-free magnetization form in magnetic alloys [42]. Specifically, we investigate three types of compatible interfaces, namely, martensite/martensite twin interfaces, an exact austenite/martensite interface, and supercompatible interfaces satisfying the cofactor conditions.

A. Martensite/martensite interfaces

Following Eq. (4), we define the three structural transformations, namely, cubic to tetragonal, cubic to trigonal, and cubic to monoclinic-I, in cubic magnetic alloys. Table I lists the corresponding strain tensors $\mathbf{E}_i$, as a function of magnetostriction constants, for each of these structural transformations. We use two variants of the strain tensor, e.g., the Ith strain variant $\mathbf{E}_I$ and the Jth strain variant $\mathbf{E}_J$, to examine whether there exist vectors $\mathbf{a} \neq 0$ and $\hat{\mathbf{n}}$ that satisfy the twinning equation (strain compatibility condition in the geometrically linear theory)

$$\mathbf{E}_I - \mathbf{E}_J = \frac{1}{2}(\mathbf{a}\otimes\hat{\mathbf{n}} + \hat{\mathbf{n}}\otimes\mathbf{a}). \quad (5)$$

Equation (5) has a solution if and only if $\mathbf{E} = \mathbf{E}_I - \mathbf{E}_J \neq 0$ and the eigenvalues of $\mathbf{E}$ satisfy $\epsilon_1 \leqslant \epsilon_2 = 0 \leqslant \epsilon_3$. From Table I, magnetic materials with the cubic-to-tetragonal transformation form compatible ferromagnetic interfaces if and only if $\lambda_{100} \neq 0$. Similarly,

TABLE I. Strain matrices $\mathbf{E}_i$ and martensite twin solutions for a ferromagnetic soft magnet with tetragonal, trigonal, and monoclinic symmetries. Twin solutions for the martensite/martensite interfaces exist for specific values of the magnetostriction constants. Here, n, number of variants.

Easy axes	Transformation	Strain tensor $\mathbf{E}_i$	Eigenvalues of $\mathbf{E}$	Solutions exist if and only if
⟨100⟩	Cubic to tetragonal $n(\mathbf{E}_i) = 3$ $n(\mathbf{E}_{i\pm}) = 6$	$\begin{bmatrix} \lambda_{100} & 0 & 0 \\ 0 & -\frac{\lambda_{100}}{2} & 0 \\ 0 & 0 & -\frac{\lambda_{100}}{2} \end{bmatrix}$	$\{-\frac{3\lambda_{100}}{2}, 0, \frac{3\lambda_{100}}{2}\}$	$\lambda_{100} \neq 0$
⟨111⟩	Cubic to trigonal $n(\mathbf{E}_i) = 4$ $n(\mathbf{E}_{i\pm}) = 8$	$\begin{bmatrix} 0 & \frac{\lambda_{111}}{2} & \frac{\lambda_{111}}{2} \\ \frac{\lambda_{111}}{2} & 0 & \frac{\lambda_{111}}{2} \\ \frac{\lambda_{111}}{2} & \frac{\lambda_{111}}{2} & 0 \end{bmatrix}$	$\{-\sqrt{2}\lambda_{111}, 0, \sqrt{2}\lambda_{111}\}$	$\lambda_{111} \neq 0$
⟨110⟩	Cubic to monoclinic $n(\mathbf{E}_i) = 6$ $n(\mathbf{E}_{i\pm}) = 12$	$\begin{bmatrix} -\frac{\lambda_{100}}{2} & 0 & 0 \\ 0 & \frac{\lambda_{100}}{4} & \frac{3\lambda_{111}}{4} \\ 0 & \frac{3\lambda_{111}}{4} & \frac{\lambda_{100}}{4} \end{bmatrix}$	$\{-\frac{3}{4}\sqrt{\lambda_{100}^2 + 2\lambda_{111}^2}, 0,$ $\frac{3}{4}\sqrt{\lambda_{100}^2 + 2\lambda_{111}^2}\}$	$\lambda_{100} \neq 0$ and $\lambda_{111} \neq 0$

magnetic alloys with the cubic-to-trigonal transformation form compatible ferromagnetic interfaces if and only if $\lambda_{111} \neq 0$. For the cubic-to-monoclinic transformation, compatible interfaces form when both $\lambda_{111} \neq 0$ and $\lambda_{100} \neq 0$ are satisfied. The resulting twin solutions for each of these structural transformations are listed as a function of magnetostriction constants in the Appendix.

Following James and Wuttig [18], we note that for typical type I or type II twins (or compound twins), mechanical compatibility at the martensite/martensite interface implies magnetic compatibility (i.e., divergence-free magnetization). Figure 2 shows representative examples of compatible interfaces constructed using Eq. (5) with divergence-free magnetization.

B. Exact austenite/martensite interface

Next, we solve the twinning equation between the austenite phase and a single variant of the martensite phase. We use the transformation strains $\mathbf{E}_i$ for the cubic-to-tetragonal, cubic-to-trigonal, and cubic-to-monoclinic transformations and examine whether there exist vectors $\mathbf{a} \neq \mathbf{0}$ and $\hat{\mathbf{n}}$ that satisfy the compatibility condition in geometrically linear theory:

$$\mathbf{E}_I - 0 = \tfrac{1}{2}(\mathbf{a} \otimes \hat{\mathbf{n}} + \hat{\mathbf{n}} \otimes \mathbf{a}). \tag{6}$$

As discussed above, Eq. (6) has a solution if and only if $\mathbf{E} = \mathbf{E}_I - 0 \neq 0$ and the eigenvalues of $\mathbf{E}$ satisfy $\epsilon_1 \leqslant \epsilon_2 = 0 \leqslant \epsilon_3$. Table II lists the eigenvalues for the matrix $\mathbf{E}$ as a function of the material's magnetostriction constants $\lambda_{100}, \lambda_{111}$ and the necessary conditions to form an exact austenite/martensite interface.

For the martensite variant with ⟨100⟩ easy axes of magnetization an exact austenite/martensite interface forms for a contradicting condition of $\lambda_{100} = 0$ and $\lambda_{100} \neq 0$. This condition is impossible for a magnetic material with one magnetostriction constant along ⟨100⟩ longitudinal directions, and thus no exact austenite/martensite interface can form in magnetic alloys transforming from a cubic paramagnet to a tetragonal ferromagnet. Similarly, for the martensite variant with ⟨111⟩ easy axes, no exact austenite/martensite interface can form in magnetic alloys transforming from a cubic paramagnet to a trigonal ferromagnet. In contrast with previous transformations, the transformation from cubic paramagnetic to monoclinic-I ferromagnetic satisfies Eq. (6) and forms an exact austenite/martensite interface for

$$\begin{aligned} &\lambda_{100} = 0 \quad \text{and} \quad \lambda_{111} \neq 0, \quad \text{or} \\ &\lambda_{100} = 3\lambda_{111} \quad \text{and} \quad \lambda_{111} \neq 0, \quad \text{or} \\ &\lambda_{100} = -3\lambda_{111} \quad \text{and} \quad \lambda_{111} \neq 0. \end{aligned} \tag{7}$$

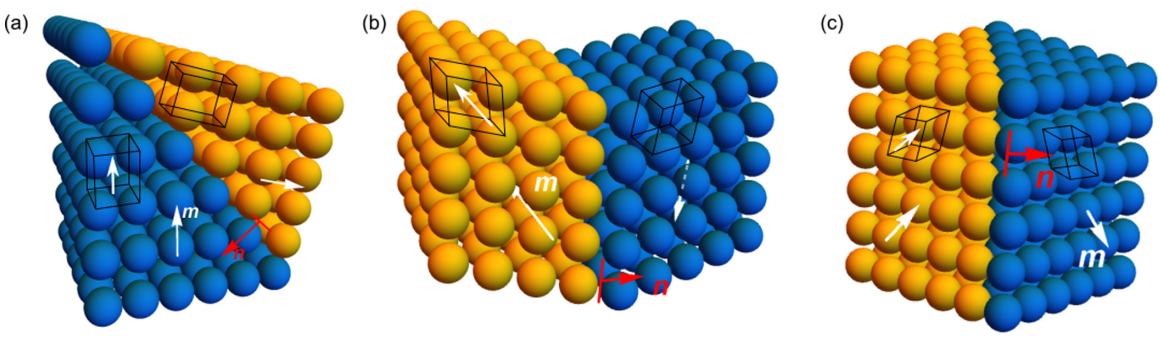

FIG. 2. Martensite/martensite interfaces in (a) tetragonal, (b) trigonal, and (c) monoclinic variants.

TABLE II. Necessary conditions for an exact interface between the cubic-paramagnetic phase and a single variant of the ferromagnetic phase. A/M, austenite/martensite.

Easy axes	Transformation	Eigenvalues of matrix $\mathbf{E} = \mathbf{E}_I - 0$	Condition for exact A/M interface
⟨100⟩	Cubic to tetragonal	$\epsilon_1 = -\frac{\lambda_{100}}{2}$ $\epsilon_2 = -\frac{\lambda_{100}}{2}$ $\epsilon_3 = \lambda_{100}$	No solution; $\epsilon_2 = 0$ if and only if $\lambda_{100} = 0$
⟨111⟩	Cubic to trigonal	$\epsilon_1 = -\frac{\lambda_{111}}{2}$ $\epsilon_2 = -\frac{\lambda_{111}}{2}$ $\epsilon_3 = \lambda_{111}$	No solution; $\epsilon_2 = 0$ if and only if $\lambda_{111} = 0$
⟨110⟩	Cubic to monoclinic	$\epsilon_1 = -\frac{\lambda_{100}}{2}$ $\epsilon_2 = \frac{1}{4}(\lambda_{100} - 3\lambda_{111})$ $\epsilon_3 = \frac{1}{4}(\lambda_{100} + 3\lambda_{111})$	Solutions exist for $\lambda_{100} \in \{0, 3\lambda_{111}, -3\lambda_{111}\}$; divergence-free interface forms for $\lambda_{100} = -3\lambda_{111}$

Figure 3 shows the combinations of magnetostriction constants $\lambda_{100}, \lambda_{111}$ for which the structural strain variants satisfy the compatibility condition in Eq. (7). Please note that Fig. 3 also shows combinations of magnetostriction constants at large values (which are likely to be unrealistic) and may fall outside the Ericksen-Pitteri neighborhood [30]; however, we retain them here for illustrative purposes. Furthermore, it is important to note that these results from the geometrically linear case should not be used for alloy development for materials with appreciable transformation strains.

We next examine whether the magnetization $\mathbf{m}$ at the exact austenite/martensite (paramagnetic/ferromagnetic) interface is divergence-free for the conditions listed in Eq. (7). That is, we check whether the following condition is true:

$$\mathbf{m} \cdot \mathbf{n} = 0. \tag{8}$$

Here, $\mathbf{m}$ is the magnetization of the monoclinic-I phase, and $\mathbf{n}$ is the normal vector of the exact paramagnetic/ferromagnetic interface.

We compute Eq. (8) for every combination of the monoclinic-I variant (12 variants) with the cubic lattice for both type I and type II solutions of Eq. (6); see Fig. 3(b). We find that not all compatible interfaces have divergence-free magnetization, and divergence-free exact interfaces form only at the $\lambda_{100} = -3\lambda_{111}$ condition. Figure 3(c) shows a representative example of a divergence-free exact interface between a monoclinic-I variant ($\mathbf{E}_4$) and a cubic lattice constructed using Eqs. (7) and (8).

C. Cofactor conditions

We investigate whether any paramagnetic and ferromagnetic variants satisfy the cofactor compatibility conditions [17]. These cofactor conditions, introduced in Ref. [17], are necessary and sufficient conditions for a given twin system to satisfy the equations of the crystallographic theory of martensite for *any* volume fraction f of the twins, $0 \leqslant f \leqslant 1$. For physical interpretation, the cofactor conditions allow for an increased number of lattice deformations that satisfy Eq. (9). Consequently, phase transformation materials that satisfy these cofactor conditions are shown to have greatly reduced hysteresis and fatigue.

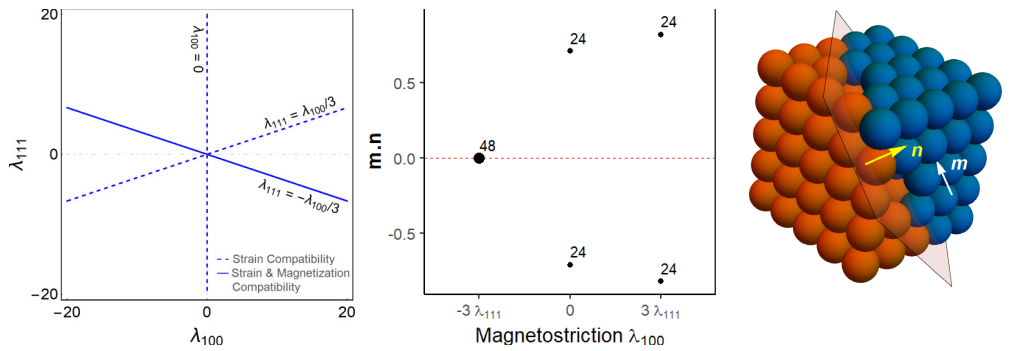

FIG. 3. (a) Combinations of magnetostriction constants $\lambda_{100}, \lambda_{111}$ for which a single ferromagnetic monoclinic variant forms an exactly compatible interface with the paramagnetic cubic lattice. Divergence-free magnetization at the exact interface is achieved only for $\lambda_{111} = -\frac{\lambda_{100}}{3}$. (b) Dot product of the monoclinic variant's magnetization $\mathbf{m}$ at the exact paramagnetic/ferromagnetic interface (with normal $\mathbf{n}$) for the three combinations of strain compatibility. The labels correspond to the number of combinations of monoclinic variants with the orientation of the twin interface (two twin solutions). (c) A geometric construction of a ferromagnetic monoclinic variant $\mathbf{E}_4$ with a paramagnetic cubic lattice. The arrows show the normal of the exact interface and the magnetization direction, respectively.

In the geometrically linear theory the crystallographic equation for the austenite/martensite-mixture interface is

$$f\mathbf{E}_J + (1-f)\mathbf{E}_I = \tfrac{1}{2}(\mathbf{p}\otimes\hat{\mathbf{q}} + \hat{\mathbf{q}}\otimes\mathbf{p}), \tag{9}$$

in which $\mathbf{E}_I, \mathbf{E}_J$ are the martensite strain tensors, $\mathbf{p}, \hat{\mathbf{q}} \in \mathbb{R}^3$ are the twin solutions, and f is the volume fraction of the martensite mixture. Following Ref. [17], we next list the theorem for cofactor conditions in the geometrically linear theory.

Theorem. Let $\mathbf{E}_I \in \mathbb{R}^{3\times3}_{\text{sym}}$ be the given strain tensor and $\hat{\mathbf{e}} \in \mathbb{R}^3$, $|\hat{\mathbf{e}}| = 1$, be the given axis of rotation. We then define another strain tensor $\mathbf{E}_J = \mathbf{Q}\mathbf{E}_I\mathbf{Q}^T$ in which $\mathbf{Q} = -\mathbf{I} + 2\hat{\mathbf{e}}\otimes\hat{\mathbf{e}}$ is the rotation matrix, such that $\mathbf{E}_J \neq \mathbf{E}_I$. The two strain tensors satisfy the linearized Hadamard jump condition with the twin solutions $\mathbf{a}, \hat{\mathbf{n}}$ defined by Eq. (5). Given the above-described conditions, there exists $\mathbf{p}, \hat{\mathbf{q}} \in \mathbb{R}^3$ satisfying Eq. (9) for every value of $0 \leqslant f \leqslant 1$ if and only if the following three cofactor conditions are satisfied.

Cofactor condition 1 (CC1) is $\epsilon_2 = 0$, i.e., the middle eigenvalues of the strain tensor $\mathbf{E}_I$ should be zero, with rank of $\mathbf{E}_I = 2$.

Cofactor condition 2 (CC2) is $(\mathbf{a}\cdot\mathbf{v}_2)(\hat{\mathbf{n}}\cdot\mathbf{v}_2) = 0$, in which vector $\mathbf{v}_2$ is the ordered middle eigenvector of $\mathbf{E}_I$, and $\mathbf{E}_I\mathbf{v}_2 = 0$, $|\mathbf{v}_2| = 1$ [43].

Cofactor condition 3 (CC3) is the inequality $[\text{tr}(\mathbf{E}_I + \mathbf{E}_J)]^2 - \text{tr}[(\mathbf{E}_I + \mathbf{E}_J)^2] \leqslant 0$.

The proof of this theorem and its physical interpretation are given in Ref. [17]. For our purposes, we note that the cofactor conditions allow for an increased number of lattice deformations that satisfy Eq. (9) without elastic energy.

We next examine whether the structural transformations described by the preferred strain matrix $\mathbf{E}_0(\mathbf{m})$ in Eq. (4) (a) satisfy the three cofactor conditions and (b) form locally divergence-free microstructures. We compute the twin solutions for each combination of ferromagnetic variants and systematically check whether they satisfy each of the three cofactor conditions, CC1–CC3. We illustrate this procedure using a representative example of a cubic-to-monoclinic-I transformation in the Appendix and present the general results below.

CC1. From Sec. III B we note that the cubic-to-monoclinic-I transformation strain alone satisfies the first cofactor condition, i.e., $\epsilon_2 = 0$, for specific combinations of magnetostriction constants, namely, $\lambda_{100} \in \{0, 3\lambda_{111}, -3\lambda_{111}\}$. However, from Figs. 3(a) and 3(b) we note that the magnetization compatibility, in addition to the strain compatibility, is achieved only for $\lambda_{100} = -3\lambda_{111}$. We next test whether the structural transformation from cubic to monoclinic-I satisfies CC2 and CC3, respectively.

CC2. A total of $n = 720$ twin solutions for monoclinic martensite variants were systematically examined to satisfy CC2 [i.e., $(\mathbf{a}\cdot\mathbf{v}_2)(\hat{\mathbf{n}}\cdot\mathbf{v}_2) = 0$] for each combination of the magnetostriction constants. Figure 4(a) shows that the second cofactor condition is satisfied only for monoclinic-I variants with magnetostriction constant $\lambda_{100} = 0$. We find that the second cofactor condition is not satisfied for other combinations of magnetostriction constants $\lambda_{100} = \pm3\lambda_{111}$.

CC3. Figure 4(b) shows that the third cofactor condition is satisfied for cubic-to-monoclinic-I transformation for all three combinations of magnetostriction constants, namely, $\lambda_{100} \in \{0, 3\lambda_{111}, -3\lambda_{111}\}$. Here, we systematically examine the condition $[\text{tr}(\mathbf{E}_I + \mathbf{E}_J)]^2 - \text{tr}[(\mathbf{E}_I + \mathbf{E}_J)^2] \leqslant 0$ for all combinations of monoclinic-I variants for each combination of the magnetostriction constants; see Fig. 4(b).

Overall, only the phase transformation from cubic (paramagnet) to monoclinic-I (ferromagnet) described by $\mathbf{E}_0(\mathbf{m})$ in Eq. (4) satisfies all cofactor conditions with $\lambda_{100} = 0$, $\lambda_{111} \neq 0$; see the Venn diagram in Fig. 4(c). However, from Sec. III B and Fig. 3(b), recall that the magnetization at the paramagnetic/ferromagnetic interface is not divergence-free at $\lambda_{100} = 0$. Consequently, the resulting austenite/martensite-mixture microstructure satisfying Eq. (9) with $\lambda_{100} = 0$ is not locally divergence-free and is energetically unfavorable. Other compatible austenite/martensite-mixture interfaces, such as the one shown in Fig. 4(d), can form during phase transformations. For example, in Fig. 4(d), a martensite mixture containing monoclinic variants $\mathbf{E}_3, \mathbf{E}_4$ separated by 180° domain walls forms a compatible interface with a cubic-austenite phase [44]. This microstructure contains an exact divergence-free interface between a ferromagnetic monoclinic-I variant $\mathbf{E}_4$ and the paramagnetic cubic lattice and thus does not have any local penalty from the demagnetization energy.

More broadly, our analysis of the cofactor conditions shows that magnetic materials that undergo cubic-to-tetragonal, cubic-to-trigonal, and cubic-to-monoclinic-I phase transformations are unlikely to form microstructures satisfying the cofactor conditions and are thus not suitable candidates to engineer highly reversible microstructures. We next investigate whether other structural transformation routes leading to lower-symmetry martensites, such as orthorhombic or monoclinic-II, can form compatible microstructures.

IV. TRANSFORMATION FROM CUBIC TO LOW-SYMMETRY STRUCTURES

Thus far, we have used the strain tensor $\mathbf{E}_0(\mathbf{m})$ in Eq. (4), which (a) describes structural transformations from a reference cubic phase (paramagnetic) to a lower-symmetry phase (ferromagnetic) and (b) has two magnetostriction constants, namely, $\lambda_{100}, \lambda_{111}$, to describe lattice deformations. This construction of the strain tensor describes limited structural transformations, e.g., cubic-tetragonal, cubic-trigonal, and cubic-monoclinic-I, and does not describe lattice deformations such as cubic-orthorhombic and cubic-monoclinic-II [45]. Moreover, in several Heusler alloys the cubic phase is ferromagnetic, and the lower-symmetry phase is paramagnetic: These magnetic and structural transformations also cannot be described using the conventional strain matrix in Eq. (4). These examples indicate a need to construct a general strain (or stretch) tensor for lattice deformation in magnetic alloys, and this is a topic of ongoing research in our group.

In this section, we study the microstructural solutions for a representative Heusler alloy, the $Ni_{45}Co_5Mn_{40}Sn_{10}$ compound [9], using the geometrically exact theory. Our analysis shows that the cubic-to-monoclinic-II transformation in $Ni_{45}Co_5Mn_{40}Sn_{10}$ has more combinations of lattice parameters (compared with cubic to monoclinic-I) that satisfy geometric compatibility to form an exact austenite/martensite interface. These multiple solutions offer more flexibility to dope a Heusler magnetic alloy to satisfy the $\lambda_2 = 1$ condition

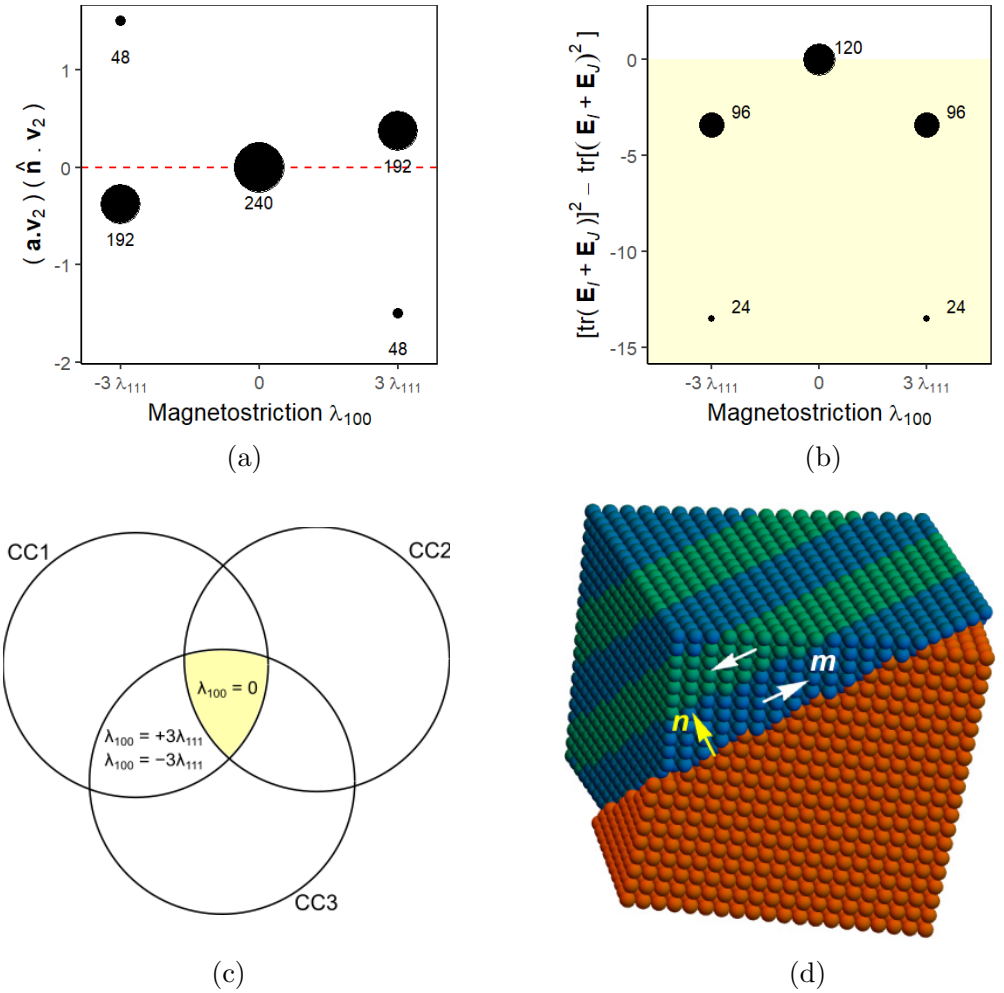

FIG. 4. (a) The second cofactor condition, $(\mathbf{a}\cdot\mathbf{v}_2)(\hat{\mathbf{n}}\cdot\mathbf{v}_2)=0$, is satisfied only for monoclinic variants with magnetostriction constants $\lambda_{100}=0$. The labels indicate the number of monoclinic variant combinations N for which the cofactor condition was systematically examined. (b) The third cofactor condition, $[\mathrm{tr}(\mathbf{E}_I+\mathbf{E}_J)]^2-\mathrm{tr}[(\mathbf{E}_I+\mathbf{E}_J)^2]\leqslant 0$, is satisfied for all three cases of magnetostriction constant, namely, $\lambda_{100}\in\{0,3\lambda_{111},-3\lambda_{111}\}$. (c) A Venn diagram showing that soft magnets with magnetostriction $\lambda_{100},\lambda_{111}\neq 0$ satisfy all three cofactor conditions. However, we know that the magnetization is not divergence-free at $\lambda_{100}=0$. (d) A geometric construction of an interface between cubic-paramagnet and monoclinic variants $\mathbf{E}_3,\mathbf{E}_4$. Note that the interface between the two monoclinic variants is a 180° wall and not a twin interface.

and/or other cofactor conditions to form highly reversible microstructures.

A. Compatible interfaces

Martensite/martensite interface. In $Ni_{45}Co_5Mn_{40}Sn_{10}$ the cubic phase is ferromagnetic, and the monoclinic-II phase (with 12 variants $\mathbf{U}_1\cdots\mathbf{U}_{12}$) is paramagnetic. This transformation differs from previously described transformations in Sec. III, in which the lower-symmetry lattice was associated with the ferromagnetic phase and the twin interfaces had to satisfy *both* strain and magnetization compatibility conditions. This condition is relaxed in $Ni_{45}Co_5Mn_{40}Sn_{10}$, in which the twin interfaces formed between different variants of the monoclinic-II phases would need to be only structurally compatible:

$$\mathbf{U}_I-\mathbf{U}_J=\mathbf{a}\otimes\hat{\mathbf{n}}. \tag{10}$$

The vectors $\mathbf{a},\hat{\mathbf{n}}$ define twin plane orientation, and $\mathbf{U}_I,\mathbf{U}_J$ are the stretch tensors in the geometrically nonlinear case. Note that each variant of the monoclinic-II phase (paramagnet) is structurally compatible with the other 11 variants via two compatible solutions. This contrasts with the martensite/martensite twins in the monoclinic-I type of ferromagnets (see Sec. III A): In this case, each variant of the monoclinic-I phase (ferromagnetic) is compatible with the other ten variants (the 11th variant has the same deformation tensor as the reference and thus cannot form a twin interface). Thus the cubic-to-monoclinic-II type of transformation generates at least two additional twin solutions when compared with the cubic-to-monoclinic-I type of transformation discussed in Sec. III.

Austenite/martensite interface. Next, we solve the twinning equation between the cubic-ferromagnetic phase (austenite) and a single variant of the monoclinic-II–paramagnetic phase (martensite). We first derive the generic condition for the cubic-to-monoclinic-II transformation using the defor-

TABLE III. Stretch tensors **U** and number of variants for magnetic alloys phase transforming to orthorhombic-I and monoclinic-II symmetries, starting with a cubic reference phase. These lower-symmetry structures have anisotropic stretches along crystallographically equivalent directions (e.g., $\alpha \neq \beta \neq \gamma$ for ⟨100⟩ directions) which cannot be described by a single magnetostriction constant λ_{100}.

Transformation	Stretch tensor **U**	Variants
Cubic to orthorhombic-I	$\begin{bmatrix} \alpha & 0 & 0 \\ 0 & \beta & 0 \\ 0 & 0 & \gamma \end{bmatrix}$	$n(\mathbf{U}_i) = 6$ $n(\mathbf{U}_{i\pm}) = 12$
Cubic to monoclinic-II	$\begin{bmatrix} \alpha & \delta & 0 \\ \delta & \beta & 0 \\ 0 & 0 & \gamma \end{bmatrix}$	$n(\mathbf{U}_i) = 12$ $n(\mathbf{U}_{i\pm}) = 24$

mation tensor in Table III and then test the compatibility condition for the $Ni_{45}Co_5Mn_{40}Sn_{10}$ alloy.

The compatibility condition in the geometrically exact theory is given by

$$\mathbf{Q}\mathbf{U}_I - \mathbf{I} = \mathbf{a} \otimes \hat{\mathbf{n}}, \tag{11}$$

in which vectors $\mathbf{a}, \hat{\mathbf{n}} \to \mathbb{R}^3$. Equation (11) has a solution if and only if the eigenvalues of $\mathbf{U}_I^2$ (or $\mathbf{U}_I$) are such that $\lambda_1 \leqslant \lambda_2 = 1 \leqslant \lambda_3$. The eigenvalues for cubic-to-monoclinic-II transformation are γ^2, $\frac{1}{2}(\alpha^2 + \beta^2 + 2\delta^2 \pm (\alpha + \beta)\sqrt{\alpha^2 - 2\alpha\beta + \beta^2 + 4\delta^2})$. Thus a magnetic alloy undergoing cubic-to-monoclinic-II transformation can form an exact austenite/martensite interface if the lattice stretches satisfy one of the conditions (for $\lambda_2 = 1$)

$$\gamma^2 = 1, \quad \text{or} \tag{12a}$$

$$\tfrac{1}{2}(\alpha^2 + \beta^2 + 2\delta^2 - (\alpha + \beta)\sqrt{\alpha^2 - 2\alpha\beta + \beta^2 + 4\delta^2}) = 1, \text{ or} \tag{12b}$$

$$\tfrac{1}{2}(\alpha^2 + \beta^2 + 2\delta^2 + (\alpha + \beta)\sqrt{\alpha^2 - 2\alpha\beta + \beta^2 + 4\delta^2}) = 1 \tag{12c}$$

and the remaining two eigenvalues satisfy $\lambda_1 \leqslant 1$ and $\lambda_3 \geqslant 1$, respectively. That is, from Eq. (12a) either a lattice stretch of $\gamma = 1$, or the balance of lattice stretches described by α, β, δ in Eqs. (12b) and (12c) should be close to 1 to form an exact interface between the cubic and monoclinic-II phases. Figure 5 shows a combination of lattice stretches for which the $\lambda_2 = 1$ condition is satisfied.

We next make a couple of observations regarding Fig. 5: First, the three-dimensional (3D) surface plot shows multiple combinations of lattice stretches for which an exact interface can form. These multiple lattice stretches increase the combination of lattice geometries that satisfy the $\lambda_2 = 1$ condition, and this condition is thus a relatively easy constraint to satisfy in experiments. This contrasts with the cubic-to-monoclinic-I transformation in Sec. III, for which the $\lambda_2 = 1$ condition is satisfied only for a specific combination of magnetostriction constants $\lambda_{100} \to 0, \pm 3\lambda_{111}$. This observation is also consistent with the fact that most experiments on phase-transforming soft magnetic alloys with $\lambda_2 = 1$ condition are materials that undergo cubic-to-monoclinic-II transformation; see Fig. 5(b). A second observation is that the majority of experimental investigations in which magnetic alloys are systematically doped to satisfy the $\lambda_2 = 1$ condition are confined to a small range of lattice stretches; see Fig. 5. While these stretches lie in the Ericksen-Pitteri neighborhood, Fig. 5(a) shows that other possible combinations of lattice deformations α, β, δ in this neighborhood could form an exact austenite/martensite interface. Broadly, Fig. 5 would serve as a quantitative guide to systematically tune alloy compositions.

For the case of the $Ni_{45}Co_5Mn_{40}Sn_{10}$ alloy, its stretch tensor satisfies Eq. (11) and thus forms a $\lambda_2 = 1$ interface. In this alloy the lattice stretches α, β, δ satisfy Eq. (12b) and thus form a compatible austenite-martensite interface. Figures 6(a) and 6(b) show an austenite/martensite interface for the cubic-monoclinic-II transformation in $Ni_{45}Co_5Mn_{40}Sn_{10}$ alloys that approximately satisfies the $\lambda_2 = 1$ condition.

Cofactor conditions. Besides the $\lambda_2 = 1$ cofactor condition, the $Ni_{45}Co_5Mn_{40}Sn_{10}$ alloy also satisfies the remaining two cofactor conditions necessary to form highly reversible microstructures; see the Appendix. These cofactor conditions are derived from the crystallographic theory of martensites [26], and materials such as the $Ni_{45}Co_5Mn_{40}Sn_{10}$ alloy that satisfy these cofactor conditions form austenite/martensite interfaces for all values of f in the range $0 \leqslant f \leqslant 1$. For

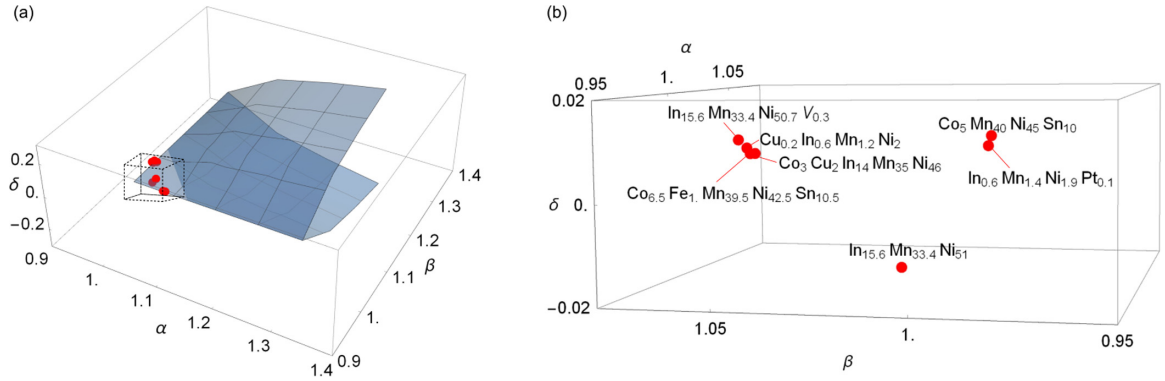

FIG. 5. (a) A 3D surface showing combinations of lattice stretches α, β, δ for the cubic-to-monoclinic-II transformation for which the $\lambda_2 = 1$ condition is satisfied. (b) Zoom of the section of the 3D plot indicated by the dashed box in (a), showing a small region of experimentally doped Heusler alloys undergoing cubic-to-monoclinic-II transformation which satisfies the $\lambda_2 = 1$ condition [9,11,36–41].

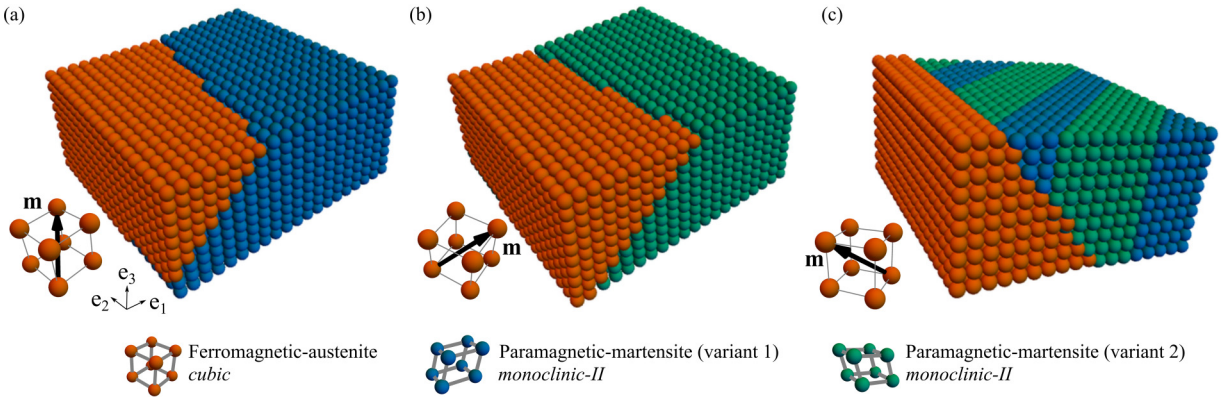

FIG. 6. Cofactor microstructures for $Ni_{45}Co_5Mn_{40}Sn_{10}$ at three representative volume fractions, (a) $f = 0$, (b) $f = 1$, and (c) $f = 3/7$. The microstructures in (a) and (b) contain an approximately ($\lambda_2 = 1.004$) compatible interface between cubic and monoclinic-II lattices (with $\mathbf{U}_1, \mathbf{U}_2$ variants). Inset sketches show the magnetization in cubic unit cells (ferromagnetic phase), and the sketches of monoclinic variants $\mathbf{U}_1, \mathbf{U}_2$ are shown in blue and green, respectively. The distortion of the monoclinic unit cells is exaggerated for illustration purposes.

example, the $Ni_{45}Co_5Mn_{40}Sn_{10}$ alloy has a solution to the equation of the crystallographic theory of martensite in the geometrically exact case for all values of the volume fraction $0 \leqslant f \leqslant 1$ (see the Appendix for further details regarding the cofactor conditions):

$$\mathbf{R}[f(\mathbf{U} + \mathbf{a} \otimes \hat{\mathbf{n}}) + (1 - f)\mathbf{U}] - \mathbf{I} = \mathbf{p} \otimes \hat{\mathbf{q}}. \quad (13)$$

Although the cofactor microstructures correspond to energy-minimizing microstructures (i.e., have vanishingly small elastic strains at the phase boundary), they are *not all* divergence-free at the paramagnetic/ferromagnetic interface. We next minimize the demagnetization energy contributions in Eq. (2) to identify structurally compatible and divergence-free paramagnetic/ferromagnetic microstructures. Specific steps followed in calculating the divergence-free microstructures are given in the Appendix, and the results are summarized in Fig. 7.

Figure 7 is a heat map of $\mathbf{m} \cdot \mathbf{K}_1$ as a function of the magnetization directions $\langle 111 \rangle$ and volume fractions f of the monoclinic-II variant mixture. The magnetization $\mathbf{m}$ in $Ni_{45}Co_5Mn_{40}Sn_{10}$ is aligned along its easy crystallographic axes $\langle 111 \rangle$ in the cubic phase, and $\mathbf{K}_1$ is the direction of the twin plane between the cubic/monoclinic-II interface. Figure 7 shows that the product $\mathbf{m} \cdot \mathbf{K}_1 \to 0$ only for specific volume fractions, e.g., $0 \leqslant f \leqslant 0.5$ for type I twins when magnetized along $[\bar{1}11, 1\bar{1}\bar{1}]$ crystallographic directions. For these volume fractions, divergence-free magnetization is obtained at the paramagnetic/ferromagnetic interface; see Figs. 6(a)–6(c). Similarly, divergence-free magnetization at the interface is observed for $0 \leqslant f \leqslant 0.5$ for type II twins when magnetized along $[\bar{1}1\bar{1}]$, $[1\bar{1}1]$ crystallographic directions. For the other combinations of volume fractions and twin plane orientations, the product $\mathbf{m} \cdot \mathbf{K}_1 \neq 0$ is not divergence-free, and these microstructures are less likely to form during phase transformations.

Overall, our microstructural analysis of magnetic materials transforming from cubic to lower-symmetry martensites (e.g., monoclinic-II) highlights the following features: First, the cubic-to-monoclinic-II structural transformation pathways offer multiple combinations of lattice parameter stretches (when compared with the finite number of solutions for the cubic-to-monoclinic-I transformation) for which an exact austenite/martensite $\lambda_2 = 1$ interface can form; see Fig. 5. These multiple solutions permit greater flex-

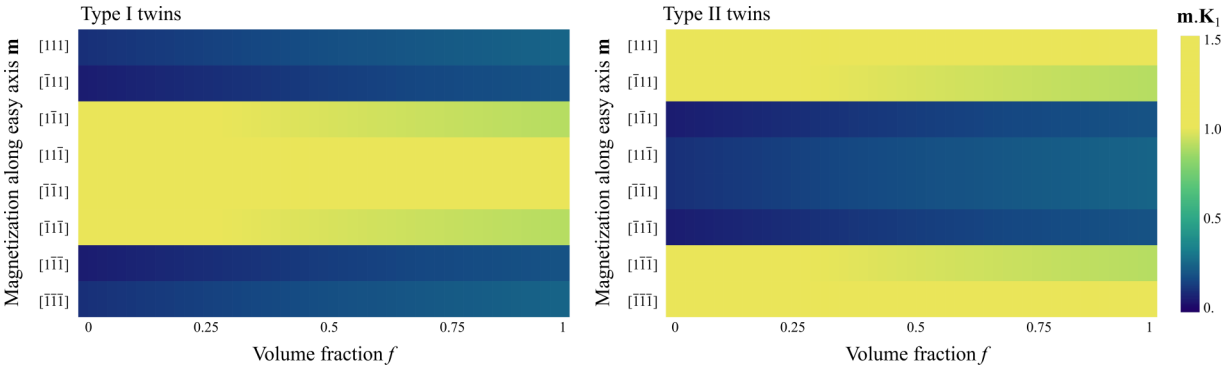

FIG. 7. A heat map of the product $\mathbf{m} \cdot \mathbf{K}_1$ for type I and type II twin solutions to Eq. (13) for $Ni_{45}Co_5Mn_{40}Sn_{10}$. The magnetization in $Ni_{45}Co_5Mn_{40}Sn_{10}$ is aligned along easy crystallographic axis $\langle 111 \rangle$, and $\mathbf{K}_1$ is the direction of the twin plane between the austenite and martensite-mixture phases with volume fraction f. Divergence-free magnetization at the interface $\mathbf{m} \cdot \mathbf{K}_1 \to 0$ is observed for $0 < f < 0.5$ at $[\bar{1}11]$, $[1\bar{1}\bar{1}]$ and $[1\bar{1}1]$, $[\bar{1}1\bar{1}]$ magnetizations in type I and type II twins, respectively.

ibility in terms of the magnetic microstructures that can form during phase transformations and thus contribute to improved reversibility of magnetic alloys. Second, phase transformations in which the lower-symmetry phase (e.g., monoclinic-II phase) is paramagnetic offer additional twin solutions, when compared with phase transformations in which the lower-symmetry phase is ferromagnetic. This is because magnetic materials in the former case would only need to satisfy the structural compatibility between nonmagnetic martensite variants. However, twin interfaces in the latter case need to be both structurally compatible and magnetically divergence-free to form energetically favorable microstructures. More broadly, our analysis suggests that magnetic materials undergoing cubic-to-monoclinic-II transformations are more suitable as candidate materials [46] that can be systematically doped to satisfy specific lattice geometries to form highly reversible magnetocaloric materials.

V. DISCUSSION

Our microstructural analysis identifies structural transformation pathways and combinations of material constants—e.g., anisotropy κ_1, magnetostriction $\lambda_{100}, \lambda_{111}$—for which magnetocaloric alloys can form highly reversible microstructures during phase transformation. We show that alloys undergoing cubic-to-monoclinic-I transformation with $\kappa_1 \leqslant 0$, $\kappa_2 \geqslant \frac{9|\kappa_1|}{4}$, and $\lambda_{111} = -\frac{\lambda_{100}}{3}$ can form exactly compatible *and* divergence-free phase boundaries. Additionally, we show that magnetic alloys with cubic-to-monoclinic-II transformation have multiple solutions satisfying the compatibility and divergence-free conditions and are suitable candidates for alloy development. In the remainder of this section, we discuss some limiting conditions of our microstructural analysis and then highlight our key findings.

Two features of this work limit the conclusions we can draw as to the microstructural solutions and the mathematical relationship between material constants for magnetic martensites. First, we derive the microstructural solutions assuming infinitesimal transformation strains in a geometrically linear framework. These solutions are not applicable to materials with appreciable strains and/or for deformations with accumulative lattice rotations. The geometrically linear strain tensor $\mathbf{E}_0(\mathbf{m})$ relates displacement gradients to the fundamental material constants (e.g., magnetostriction $\lambda_{100}, \lambda_{111}$ and magnetization $\mathbf{m}$) and thus provides an important link in deriving compatible microstructures as a function of magnetic material constants. At present, we do not know the equivalent deformation tensor (as a function of material constants) in the geometrically nonlinear theory, and this is a potential direction for future research. Second, in our microstructural analysis we assume a single-crystal magnetic body to be free from defects and to have a suitable ellipsoidal geometry. This construction satisfies a locally divergence-free condition, and the microstructures evolve to minimize the elastic and magnetocrystalline-anisotropy energies of the system. However, in the presence of defects, microstructures would need to minimize the local demagnetization energy, in addition to the elastic and anisotropy energies, and the resulting microstructural patterns may not always lead to compatible interfaces. With these reservations in mind we next discuss the impact of our analysis in terms of the magnetic alloy development program.

A key feature of our work is that we demonstrate that magnetic martensites undergoing cubic-to-monoclinic-I structural transformation [as described by $\mathbf{E}_0(\mathbf{m})$] can form structurally compatible and divergence-free $\lambda_2 = 1$ interfaces. These magnetic alloys satisfying a specific combination of material constants, namely, $\kappa_1 \leqslant 0$, $\frac{9|\kappa_1|}{4} \leqslant \kappa_2 \leqslant \infty$, $\lambda_{111} = -\frac{\lambda_{100}}{3}$, can form a perfectly compatible paramagnetic/ferromagnetic interface. An analogous interface in shape-memory alloys (another phase transformation material), formed between the austenite and martensite phases, is shown to dramatically lower thermal hysteresis. While other magnetic alloys (e.g., undergoing cubic-to-tetragonal or cubic-to-trigonal structural transformations) form compatible and divergence-free twin interfaces with martensite variants, they cannot form a divergence-free exactly compatible paramagnetic/ferromagnetic interface. Consequently, in these magnetic alloys, stressed phase boundaries could be expected to form. Our analysis of magnetic constants identifies candidate magnetocaloric alloys with specific magnetostriction and anisotropy constants that can be further doped to form highly reversible microstructures.

Another significant feature of our work is that we show that magnetic alloys with transformation pathways, such as cubic to orthorhombic or cubic to monoclinic-II, and/or magnetic alloys with a ferromagnetic-cubic phase have multiple solutions for divergence-free and exactly compatible interfaces (i.e., $\lambda_2 = 1$). For example, the transformation from ferromagnetic cubic to paramagnetic monoclinic-II in $Ni_{45}Co_5Mn_{40}Sn_{10}$ alloys can form exactly compatible and divergence-free phase boundaries for multiple combinations of lattice parameter stretches satisfying Eqs. (12a)–(12c). This contrasts with a rather rigid constraint of $\lambda_{111} = -\frac{\lambda_{100}}{3}$ for magnetic alloys with cubic-to-monoclinic-I transformation, for which finite (or fewer) combinations of lattice parameters exist. The increased number of lattice deformations satisfying Eqs. (12a)–(12c) is thus a relatively easier constraint to satisfy in alloy development experiments and is consistent with reported experimental observations. Furthermore, the cubic-to-orthorhombic and cubic-to-monoclinic-II transformations suggest that more than two magnetostriction constants are necessary to describe lattice deformations in $\mathbf{E}_0(\mathbf{m})$ and lead to open questions as to the general form of a coupled strain tensor.

Overall, our analytical results serve as a quantitative guide for developing magnetic alloys with high reversibility. The derived conditions for structural compatibility and divergence-free magnetization at the phase boundaries would be most relevant to magnetic alloys with small transformation strains.

VI. CONCLUSION

In conclusion, the present findings provide fundamental insights into how magnetic material constants, such as magnetocrystalline-anisotropy and magnetostriction constants, affect the phase transformation microstructures. We propose a mathematical relationship between material con-

TABLE IV. Notations and description of symbols used in this paper.

Notation	Description
κ_1, κ_2	Magnetocrystalline-anisotropy constants associated with the turning of the magnetization of a domain away from the easy axes of magnetization
λ_{100}, λ_{111}	Magnetostriction constants in the [100] and [111] directions of a cubic crystal representing the relative change in length of the material
θ_0	Curie temperature or phase transformation temperature
m_s	Saturation magnetization in the ferromagnetic phase
A	Gradient energy (or exchange energy) coefficient
μ_0	Vacuum permeability constant
$\zeta_{\mathbf{m}}$	Magnetostatic potential
$\mathcal{E}$	An ellipsoid magnetic body occupying a region $\mathcal{E}$
$\mathbb{R}^3$	Three-dimensional space
$\mathbf{x}$	Position of a point in the reference configuration
$\mathbf{y}$	Position of a point in the deformed configuration
$\mathbf{u}$	Displacement
$\mathbf{H}$	Displacement gradient
$\mathbf{E}$	Infinitesimal strain matrix
$\mathbf{E}$	Infinitesimal rotation matrix
$\mathbf{E}_0$	Spontaneous (or preferred) strain matrix
$\mathbf{F}$	Deformation gradient
$\mathbf{U}$	Stretch matrix (positive-definite and symmetric)
$\mathbf{Q}$ or $\mathbf{R}$	Rotation matrix
$\mathbf{I}$	Identity matrix
$\mathbf{m}$	Nondimensionalized magnetization, $\mathbf{m} = \frac{\mathbf{M}}{m_s}$
$\mathbf{H}_{\mathrm{d}}$	Demagnetization field
$(\mathbf{a}, \hat{\mathbf{n}})$ or $(\mathbf{p}, \hat{\mathbf{q}})$	Vectors describing the twin solutions
$\mathbf{K}_1$	Twin plane
ϵ_1, ϵ_2, ϵ_3	Eigenvalues of the strain matrix
$\mathbf{v}_1$, $\mathbf{v}_2$, $\mathbf{v}_3$	Eigenvectors of the strain matrix
λ_1, λ_2, λ_3	Eigenvalues of the stretch matrix
f	Volume fraction of the martensite mixture $0 \leqslant f \leqslant 1$
α, β, γ, δ	Scalar constants describing the stretch ratios between the reference and deformed lattices

stants, $\kappa_1 \leqslant 0$, $\kappa_2 \geqslant \frac{9|\kappa_1|}{4}$, and $\lambda_{111} = -\frac{\lambda_{100}}{3}$, for which exactly compatible and divergence-free phase boundaries can form in magnetic materials. Furthermore, we identify that magnetic materials undergoing cubic-to-monoclinic-II transformation have multiple solutions satisfying the high-reversibility condition and are suitable candidates for alloy development. Broadly, our findings are in a form that is amenable to alloy development, as in related searches for novel phase transformation magnetic materials with low thermal hysteresis and high reversibility.

ACKNOWLEDGMENTS

I wish to acknowledge the Provost Assistant Professor fellowship and Gabilan WiSE fellowship for providing the necessary resources to pursue this research. I would like to thank Dr. Nils Reimer (University of Southern California) for constant support and encouragement.

APPENDIX

In Table IV, a description of the symbols used in this paper is given; definitions of terminologies used in this paper can be found in Table V.

1. Linearized kinematics

Following Ref. [27,31], let us consider a body $\mathcal{E} \in \mathbb{R}^3$ undergoing a deformation $\mathbf{y} : \mathcal{E} \to \mathbb{R}^3$. We can define the displacement of a point on this body at $\mathbf{x}$ with reference to its initial position as

$$\mathbf{u}(\mathbf{x}) = \mathbf{y}(\mathbf{x}) - \mathbf{x}. \tag{A1}$$

The displacement gradient $\mathbf{H} = \nabla\mathbf{u}(\mathbf{x})$ and the deformation gradient $\mathbf{F} = \nabla\mathbf{y}(\mathbf{x})$ are related as

$$\mathbf{H}(\mathbf{x}) = \mathbf{F}(\mathbf{x}) - \mathbf{I}. \tag{A2}$$

Here, $\mathbf{I}$ is a 3×3 identity matrix. Let us next compute the strain of an infinitesimal line element oriented in the direction of the $\hat{\mathbf{e}}$ vector. Using Eq. (A2), we have

$$\text{strain} = (\sqrt{\hat{\mathbf{e}} \cdot (\mathbf{F}^{\mathrm{T}}\mathbf{F})\hat{\mathbf{e}}}) - 1 = (\sqrt{\hat{\mathbf{e}} \cdot ((\mathbf{H}+\mathbf{I})^{\mathrm{T}}(\mathbf{H}+\mathbf{I}))\hat{\mathbf{e}}}) - 1. \tag{A3}$$

Following the geometrically linear theory, for infinitesimally small strains, Eq. (A3) is approximated as

$$\text{strain} \approx (\sqrt{\hat{\mathbf{e}} \cdot (\mathbf{I} + \mathbf{H} + \mathbf{H}^{\mathrm{T}})\hat{\mathbf{e}}}) - 1 \approx \sqrt{\hat{\mathbf{e}} \cdot \left(\frac{1}{2}(\mathbf{H} + \mathbf{H}^{\mathrm{T}})\right)\hat{\mathbf{e}}}. \tag{A4}$$

TABLE V. Definitions of terminologies used in this paper.

Terminology	Definition
Diffusionless phase transformation	This is a solid-to-solid phase transformation in which the lattice structure of the material changes abruptly. There is a significant distortion of unit cells; however, there is no diffusion of atoms during this transformation (i.e., the relative position of atoms does not change). Structural materials, such as the shape-memory alloys, undergo these diffusionless phase transformations on heating or cooling of the material.
Austenite	This is the high-temperature phase of the material, often characterized by a high-symmetry lattice (e.g., cubic symmetry), is called the austenite phase. This terminology was originally used to describe the high-temperature phase of iron (and steel) and is now commonly used to describe the high-temperature phase of phase transformation materials. In this paper, we refer to the paramagnetic (i.e., high-temperature) phase as the austenite phase.
Martensite	This is the low-temperature phase of the material, often characterized by a low-symmetry lattice (e.g., tetragonal or monoclinic), is called the martensite phase. In this paper, we refer to the ferromagnetic (i.e., low-temperature) phase as the martensite phase.
Twin interface	This is a boundary formed between two separate crystals (or lattice variants) that are mirror images of each other. These interfaces are energy-minimizing deformations and are commonly observed in phase transformation materials.
Austenite/martensite interface	During phase transformation, both the austenite and martensite phases coexist in the material. The interface formed between these phases is characterized by the presence of a finely twinned martensite mixture with a uniform austenite phase. This microstructure is referred to as the austenite/martensite interface and is widely observed in phase transformation materials [31].
$\lambda_2 = 1$ condition	This is a quantitative design principle according to which a phase transformation material forms a stress-free interface (or an exactly compatible interface) between the austenite and martensite phases. Here, λ_2 is the middle eigenvalue of the stretch matrix. The $\lambda_2 = 1$ represents no relative stretch between neighboring lattices' edges during phase transformation.
Cofactor conditions	These are conditions of compatibility for which a phase transformation material forms a highly reversible microstructure [17].
Magnetocrystalline anisotropy	This material constant is associated with turning the magnetization of a domain out of the direction of easy axes.
Magnetostriction	This refers to the change in dimensions of a magnetic material under an applied magnetic field. The magnetostriction constants λ_{100} and λ_{111} represent strains along crystallographic directions $\langle 100 \rangle$ and $\langle 111 \rangle$, respectively.
Cauchy-Born rule	This is a basic hypothesis (or a rule) used in the mathematical formulation of solid mechanics which relates the movement of atoms in a crystal to the overall deformation of the bulk solid.

The strain tensor for materials with small deformations satisfying Eq. (A4) is described as the symmetric part of the displacement gradient. Deformations of several ferromagnetic materials with small magnetostriction constants can be described using Eq. (A4).

2. Energy density

The paramagnetic phase is stable at high temperatures, and the ferromagnetic phase is stable at low temperatures. Consequently, the free-energy function in Eqs. (1c) and (2) has a multiwell energy landscape shown schematically in Fig. 8. At high temperatures, the paramagnetic phase with magnetization $\mathbf{m} = 0$ and strain $\mathbf{E} = 0$ minimizes the free-energy function, i.e., $\psi(\mathbf{m} = 0, \mathbf{E} = 0) \leqslant \psi(\mathbf{m}, \mathbf{E})$. At low temperatures, the ferromagnetic phase with magnetization $\mathbf{m}_i$ and strain $\mathbf{E}_i$ minimizes the free-energy function, i.e., $\psi(\mathbf{m}_i = 0, \mathbf{E}_i = 0) \leqslant \psi(\mathbf{m}, \mathbf{E})$ corresponding to the ith ferromagnetic variant. At the phase transformation temperature $\theta = \theta_0$, the magnetization and strain are equally minimized by both the paramagnetic and ferromagnetic phases, and thus $\psi(\mathbf{m} = 0, \mathbf{E} = 0) = \psi(\mathbf{m}_1, \mathbf{E}_1) = \psi(\mathbf{m}_2, \mathbf{E}_2)$.

Let us consider a nondimensional form of the micromagnetic energy by dividing it by $\mu_0 m_s^2$, in which μ_0 and m_s correspond to the permeability constant and saturation magnetization of the material. The nondimensional form of the

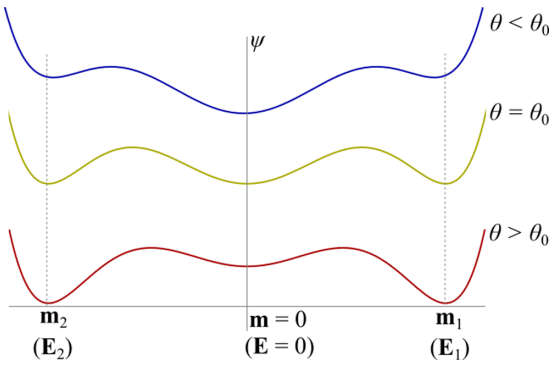

FIG. 8. Schematic illustration of a multiwell energy potential ψ for a magnetic material undergoing paramagnetic-to-ferromagnetic phase transformation. Here, $\mathbf{m}$ is the nondimensionalized magnetization, $\mathbf{E}$ is the strain tensor, and θ is the temperature.

TABLE VI. Strain variants for an alloy undergoing transformation from cubic (paramagnetic) to tetragonal (ferromagnetic). The easy axes of magnetization are along the ⟨100⟩ crystallographic directions.

Easy axes	Magnetization	Transformation strain
⟨100⟩	$\mathbf{m}=\mathbf{e}_1$	$\mathbf{E}_1=\begin{bmatrix}\lambda_{100} & 0 & 0\\ 0 & -\frac{\lambda_{100}}{2} & 0\\ 0 & 0 & -\frac{\lambda_{100}}{2}\end{bmatrix}$
	$\mathbf{m}=\mathbf{e}_2$	$\mathbf{E}_2=\begin{bmatrix}-\frac{\lambda_{100}}{2} & 0 & 0\\ 0 & \lambda_{100} & 0\\ 0 & 0 & -\frac{\lambda_{100}}{2}\end{bmatrix}$
	$\mathbf{m}=\mathbf{e}_3$	$\mathbf{E}_3=\begin{bmatrix}-\frac{\lambda_{100}}{2} & 0 & 0\\ 0 & -\frac{\lambda_{100}}{2} & 0\\ 0 & 0 & \lambda_{100}\end{bmatrix}$

micromagnetic energy is

$$\ominus_{\mathrm{N}}=\int_{\mathcal{E}'}\left\{\frac{A}{\mu_0 m_s^2}\nabla\mathbf{m}\cdot\nabla\mathbf{m}+\frac{1}{\mu_0 m_s^2}\psi(\mathbf{m},\mathbf{E},\theta)\right\}d\mathbf{x}+\frac{1}{2m_s^2}\int_{\mathbb{R}^3}\left|\nabla\zeta_{\mathbf{m}}\right|^2 d\mathbf{x}. \tag{A5}$$

Assuming typical values of the material constants for ferromagnetic material, e.g., a gradient energy coefficient of $A\sim 10^{-13}$ J/m^3, an anisotropy constant of $\kappa_1\sim 10^3$–10^5 N/m^2, a saturation magnetization of $m_s\sim 10^6$ A/m, and a permeability constant of $\mu_0\sim 1.3\times 10^{-6}$ N/A^2, we have the typical nondimensional values of the coefficients to Eq. (2):

$$\frac{A}{\mu_0 m_s^2}\sim 10^{-17},\quad \frac{\kappa_1}{\mu_0 m_s^2}\sim 10^{-3},\quad \frac{1}{m_s^2}\nabla\zeta_{\mathbf{m}}^2\sim 1. \tag{A6}$$

These ranges of values for the micromagnetic coefficients suggest that the bulk energy and the demagnetization energy are dominant and that the order of magnitude of the gradient energy does not significantly affect large-scale micromagnetic calculations. Consequently, we neglect the contribution of the gradient energy coefficients in the microstructural analysis.

The paramagnetic-to-ferromagnetic phase transformation is often a crystal-symmetry-lowering transformation. In Tables VI–VIII we list different the strain variants for the cubic-to-tetragonal, cubic-to-trigonal, and cubic-to-monoclinic-I structural transformation pathways.

3. Twin interfaces

Table IX lists the solutions to the kinematic compatibility condition for the three types of structural transformation pathways considered in Sec. III.

4. Cofactor conditions for geometrically linear theory

Below we illustrate the step-by-step procedure to compute the cofactor conditions (geometrically linear theory) using a representative cubic-to-monoclinic-I transformation pathway.

Let $\mathbf{E}_1$, $\mathbf{E}_3$ be two monoclinic variants that are given by

$$\mathbf{E}_1=\begin{bmatrix}-\frac{\lambda_{100}}{2} & 0 & 0\\ 0 & \frac{\lambda_{100}}{4} & \frac{3\lambda_{111}}{4}\\ 0 & \frac{3\lambda_{111}}{4} & \frac{\lambda_{100}}{4}\end{bmatrix},$$

$$\mathbf{E}_3=\begin{bmatrix}-\frac{\lambda_{100}}{2} & 0 & 0\\ 0 & \frac{\lambda_{100}}{4} & -\frac{3\lambda_{111}}{4}\\ 0 & -\frac{3\lambda_{111}}{4} & \frac{\lambda_{100}}{4}\end{bmatrix}.$$

The two strain tensors are related by a rotation $\mathbf{Q}$ about the axis

$$\hat{\mathbf{e}}=\begin{pmatrix}0\\1\\0\end{pmatrix}, \tag{A7}$$

TABLE VII. Strain variants for an alloy undergoing transformation from cubic (paramagnetic) to trigonal (ferromagnetic). The easy axes of magnetization are along the ⟨111⟩ crystallographic directions.

Easy axes	Magnetization	Transformation strain
⟨111⟩	$\mathbf{m}=\pm\frac{1}{\sqrt{3}}(\mathbf{e}_1+\mathbf{e}_2+\mathbf{e}_3)$	$\mathbf{E}_1=\begin{bmatrix}0 & \frac{\lambda_{111}}{2} & \frac{\lambda_{111}}{2}\\ \frac{\lambda_{111}}{2} & 0 & \frac{\lambda_{111}}{2}\\ \frac{\lambda_{111}}{2} & \frac{\lambda_{111}}{2} & 0\end{bmatrix}$
	$\mathbf{m}=\pm\frac{1}{\sqrt{3}}(-\mathbf{e}_1+\mathbf{e}_2+\mathbf{e}_3)$	$\mathbf{E}_2=\begin{bmatrix}0 & -\frac{\lambda_{111}}{2} & -\frac{\lambda_{111}}{2}\\ -\frac{\lambda_{111}}{2} & 0 & \frac{\lambda_{111}}{2}\\ -\frac{\lambda_{111}}{2} & \frac{\lambda_{111}}{2} & 0\end{bmatrix}$
	$\mathbf{m}=\pm\frac{1}{\sqrt{3}}(\mathbf{e}_1-\mathbf{e}_2+\mathbf{e}_3)$	$\mathbf{E}_3=\begin{bmatrix}0 & -\frac{\lambda_{111}}{2} & \frac{\lambda_{111}}{2}\\ -\frac{\lambda_{111}}{2} & 0 & -\frac{\lambda_{111}}{2}\\ \frac{\lambda_{111}}{2} & -\frac{\lambda_{111}}{2} & 0\end{bmatrix}$
	$\mathbf{m}=\pm\frac{1}{\sqrt{3}}(\mathbf{e}_1+\mathbf{e}_2-\mathbf{e}_3)$	$\mathbf{E}_4=\begin{bmatrix}0 & \frac{\lambda_{111}}{2} & -\frac{\lambda_{111}}{2}\\ \frac{\lambda_{111}}{2} & 0 & -\frac{\lambda_{111}}{2}\\ -\frac{\lambda_{111}}{2} & -\frac{\lambda_{111}}{2} & 0\end{bmatrix}$

TABLE VIII. Strain variants for an alloy undergoing transformation from cubic (paramagnetic) to monoclinic-I (ferromagnetic). The easy axes of magnetization are along the ⟨110⟩ crystallographic directions.

Easy axes	Magnetization	Transformation strain
⟨110⟩	$\mathbf{m} = \pm\frac{1}{\sqrt{2}}(\mathbf{e}_2 + \mathbf{e}_3)$	$\mathbf{E}_1 = \begin{bmatrix} -\frac{\lambda_{100}}{2} & 0 & 0 \\ 0 & \frac{\lambda_{100}}{4} & \frac{3\lambda_{111}}{4} \\ 0 & \frac{3\lambda_{111}}{4} & \frac{\lambda_{100}}{4} \end{bmatrix}$
	$\mathbf{m} = \pm\frac{1}{\sqrt{2}}(\mathbf{e}_2 - \mathbf{e}_3)$	$\mathbf{E}_2 = \begin{bmatrix} -\frac{\lambda_{100}}{2} & 0 & 0 \\ 0 & \frac{\lambda_{100}}{4} & -\frac{3\lambda_{111}}{4} \\ 0 & -\frac{3\lambda_{111}}{4} & \frac{\lambda_{100}}{4} \end{bmatrix}$
	$\mathbf{m} = \pm\frac{1}{\sqrt{2}}(\mathbf{e}_1 + \mathbf{e}_3)$	$\mathbf{E}_3 = \begin{bmatrix} \frac{\lambda_{100}}{4} & 0 & \frac{3\lambda_{111}}{4} \\ 0 & -\frac{\lambda_{100}}{2} & 0 \\ \frac{3\lambda_{111}}{4} & 0 & \frac{\lambda_{100}}{4} \end{bmatrix}$
	$\mathbf{m} = \pm\frac{1}{\sqrt{2}}(\mathbf{e}_1 - \mathbf{e}_3)$	$\mathbf{E}_4 = \begin{bmatrix} \frac{\lambda_{100}}{4} & 0 & -\frac{3\lambda_{111}}{4} \\ 0 & -\frac{\lambda_{100}}{2} & 0 \\ -\frac{3\lambda_{111}}{4} & 0 & \frac{\lambda_{100}}{4} \end{bmatrix}$
	$\mathbf{m} = \pm\frac{1}{\sqrt{2}}(\mathbf{e}_1 + \mathbf{e}_2)$	$\mathbf{E}_5 = \begin{bmatrix} \frac{\lambda_{100}}{4} & \frac{3\lambda_{111}}{4} & 0 \\ \frac{3\lambda_{111}}{4} & \frac{\lambda_{100}}{4} & 0 \\ 0 & 0 & -\frac{\lambda_{100}}{2} \end{bmatrix}$
	$\mathbf{m} = \pm\frac{1}{\sqrt{2}}(\mathbf{e}_1 - \mathbf{e}_2)$	$\mathbf{E}_6 = \begin{bmatrix} \frac{\lambda_{100}}{4} & -\frac{3\lambda_{111}}{4} & 0 \\ -\frac{3\lambda_{111}}{4} & \frac{\lambda_{100}}{4} & 0 \\ 0 & 0 & -\frac{\lambda_{100}}{2} \end{bmatrix}$

and the rotation matrix is given by

$$\mathbf{Q} = -\mathbf{I} + 2\hat{\mathbf{e}} \otimes \hat{\mathbf{e}} = \begin{bmatrix} -1 & 0 & 0 \\ 0 & 1 & 0 \\ 0 & 0 & -1 \end{bmatrix}. \tag{A8}$$

Using Eqs. (A7) and (A8), we can verify that $\mathbf{E}_3 = \mathbf{Q}\mathbf{E}_1\mathbf{Q}^T$. The two strain tensors fit compatibly to form a twin interface with solutions given in Table IX. To illustrate our calculation, we consider a candidate twin solution:

$$\mathbf{a} = 4((\hat{\mathbf{e}} \cdot \mathbf{E}\hat{\mathbf{e}}) - \mathbf{E}\hat{\mathbf{e}}) = -3\lambda_{111}\hat{\mathbf{e}}_3, \mathbf{n} = \hat{\mathbf{e}} = \hat{\mathbf{e}}_2. \tag{A9}$$

Next we examine whether the monoclinic variants $\mathbf{E}_1, \mathbf{E}_3$ satisfy cofactor conditions to form a phase boundary with zero elastic energy. We set $\mathbf{E}_I = \mathbf{E}_1$ and $\mathbf{E}_J = \mathbf{E}_3$ and check CC1–CC3 systematically.

(1) The eigenvalues of $\mathbf{E}_I = \mathbf{E}_1$ are $\{\frac{-\lambda_{100}}{2}, \frac{1}{4}(\lambda_{100} - 3\lambda_{111}), \frac{1}{4}(\lambda_{100} + 3\lambda_{111})\}$. CC1 is satisfied if and only if $\lambda_{100} = 0$, or $\lambda_{100} = 3\lambda_{111}$, or $\lambda_{100} = -3\lambda_{111}$. Using these combinations of the magnetostriction constant, we next check for CC2 and CC3.

(2) We next check CC2 for each combination of the magnetostriction values: (i) If $\lambda_{100} = 0$, we have $\epsilon_2 = 0$,

TABLE IX. Strain matrices $\mathbf{E}_i$ and martensite twin solutions for a ferromagnetic soft magnet with tetragonal, trigonal, and monoclinic symmetries. Twin solutions for the martensite/martensite interfaces exist for specific values of the magnetostriction constants.

Easy axes	Transformation	Strain tensor	Solutions exist if and only if	Martensite/martensite twins
⟨100⟩	Cubic to tetragonal $n(\mathbf{E}_i) = 3$ $n(\mathbf{E}_{i\pm}) = 6$	$\begin{bmatrix} \lambda_{100} & 0 & 0 \\ 0 & -\frac{\lambda_{100}}{2} & 0 \\ 0 & 0 & -\frac{\lambda_{100}}{2} \end{bmatrix}$	$\lambda_{100} \neq 0$	Compound $\mathbf{a} = \frac{3}{\sqrt{2}}\lambda_{100}(-\hat{\mathbf{e}}_1+\hat{\mathbf{e}}_2)$ $\hat{\mathbf{n}} = \frac{1}{\sqrt{2}}(\hat{\mathbf{e}}_1+\hat{\mathbf{e}}_2)$ $\mathbf{a} = \frac{3}{\sqrt{2}}\lambda_{100}(\hat{\mathbf{e}}_1+\hat{\mathbf{e}}_2)$ $\hat{\mathbf{n}} = \frac{1}{\sqrt{2}}(-\hat{\mathbf{e}}_1+\hat{\mathbf{e}}_2)$
⟨111⟩	Cubic to trigonal $n(\mathbf{E}_i) = 4$ $n(\mathbf{E}_{i\pm}) = 8$	$\begin{bmatrix} 0 & \frac{\lambda_{111}}{2} & \frac{\lambda_{111}}{2} \\ \frac{\lambda_{111}}{2} & 0 & \frac{\lambda_{111}}{2} \\ \frac{\lambda_{111}}{2} & \frac{\lambda_{111}}{2} & 0 \end{bmatrix}$	$\lambda_{111} \neq 0$	Compound $\mathbf{a} = 2\sqrt{2}\lambda_{111}(\hat{\mathbf{e}}_1)$ $\hat{\mathbf{n}} = \frac{-1}{\sqrt{2}}(\hat{\mathbf{e}}_2+\hat{\mathbf{e}}_3)$ $\mathbf{a} = 2\lambda_{111}(\hat{\mathbf{e}}_2+\hat{\mathbf{e}}_3)$ $\hat{\mathbf{n}} = (\hat{\mathbf{e}}_1)$
⟨110⟩	Cubic to monoclinic $n(\mathbf{E}_i) = 6$ $n(\mathbf{E}_{i\pm}) = 12$	$\begin{bmatrix} -\frac{\lambda_{100}}{2} & 0 & 0 \\ 0 & \frac{\lambda_{100}}{4} & \frac{3\lambda_{111}}{4} \\ 0 & \frac{3\lambda_{111}}{4} & \frac{\lambda_{100}}{4} \end{bmatrix}$	$\lambda_{100} \neq 0$ and $\lambda_{111} \neq 0$	Compound $\mathbf{a} = -3\lambda_{111}\hat{\mathbf{e}}_3$ $\hat{\mathbf{n}} = \hat{\mathbf{e}}_2$ $\mathbf{a} = 3\lambda_{111}\hat{\mathbf{e}}_2$ $\hat{\mathbf{n}} = -\hat{\mathbf{e}}_3$

and the corresponding middle eigenvector is given by $\mathbf{v}_2 = (1 \quad 0 \quad 0)^{\mathrm{T}}$. This eigenvector satisfies $\mathbf{E}_I\mathbf{v}_2 = 0$, $|\mathbf{v}_2| = 1$, and $(\mathbf{a}\cdot\mathbf{v_2})(\mathbf{n}\cdot\mathbf{v_2}) = (-3\lambda_{111}\hat{\mathbf{e}}_3\cdot\mathbf{v}_2)(\hat{\mathbf{e}}_2\cdot\mathbf{v}_2) = 0$. Thus with $\lambda_{100} = 0$, $\mathbf{E}_1, \mathbf{E}_3$ satisfy CC2. (ii) If $\lambda_{100} = \pm 3\lambda_{111}$ and $\lambda_{111} \neq 0$, we have the middle eigenvalue $\epsilon_2 = 0$ and the corresponding eigenvector given by $\mathbf{v}_2 = \frac{1}{\sqrt{2}}(0 \quad -1 \quad 1)^{\mathrm{T}}$. This eigenvector satisfies $\mathbf{E}_I\mathbf{v}_2 = 0$ and $|\mathbf{v}_2| = 1$; however, it does not satisfy the condition $(\mathbf{a}\cdot\mathbf{v_2})(\mathbf{n}\cdot\mathbf{v_2}) = \frac{3}{\sqrt{2}}\lambda_{111} \neq 0$. Thus with $\lambda_{100} = \pm 3\lambda_{111}$, $\mathbf{E}_1, \mathbf{E}_3$ do not satisfy CC2.

(3) We check CC3 for each combination of the magnetostriction values: (i) The inequality $\mathrm{tr}(\mathbf{E}_I + \mathbf{E}_J)^2 + \mathrm{tr}[(\mathbf{E}_I + \mathbf{E}_J)^2] = \frac{-3\lambda_{100}^2}{2} \leqslant 0$ if and only if $\lambda_{100} = 0$. Thus with $\lambda_{100} = 0$, $\mathbf{E}_1, \mathbf{E}_3$ satisfy CC3. (ii) The inequality $\mathrm{tr}(\mathbf{E}_I + \mathbf{E}_J)^2 + \mathrm{tr}[(\mathbf{E}_I + \mathbf{E}_J)^2] = \frac{-3\lambda_{100}^2}{2} = \frac{-27\lambda_{111}^2}{2} \leqslant 0$. Thus with $\lambda_{100} = \pm 3\lambda_{111}$, $\mathbf{E}_1, \mathbf{E}_3$ satisfies CC3.

We repeat this procedure (steps 1–3), starting with different combinations of monoclinic variants and systematically examine whether they satisfy the cofactor conditions.

5. Cofactor conditions for the geometrically exact theory

Following Ref. [3], we list the cofactor conditions (geometrically exact theory) that are necessary and sufficient for Eq. (13) to have a solution for all values of the volume fraction $0 \leqslant f \leqslant 1$.

Theorem. Let $\mathbf{U} \in \mathbb{R}^{3\times3}_{+\mathrm{sym}}$ be the given stretch tensor and $\hat{\mathbf{U}} = (-\mathbf{I} + 2\hat{\mathbf{e}}\otimes\hat{\mathbf{e}})\mathbf{U}(-\mathbf{I} + 2\hat{\mathbf{e}}\otimes\hat{\mathbf{e}})$ for some $|\hat{\mathbf{e}}| = 1$, so that there exist $\hat{\mathbf{R}} \in \mathrm{SO}(3)$ and $\mathbf{a}, \hat{\mathbf{n}} \in \mathbb{R}^3$ such that $\hat{\mathbf{R}}\hat{\mathbf{U}} = \mathbf{U} + \mathbf{a}\otimes\hat{\mathbf{n}}$. Assuming that $\mathbf{a} \neq 0, \hat{\mathbf{n}} \neq 0$, Eq. (13) has solutions $\mathbf{R} \in \mathrm{SO}(3)$, $\mathbf{p}$, $\hat{\mathbf{q}}$ for each $f \in [0, 1]$, if and only if the following cofactor conditions are satisfied:

$$\lambda_2 = 0, \quad \text{i.e., the middle eigenvalue of } \mathbf{U};$$

$$\mathbf{a}\cdot\mathbf{U}\mathrm{cof}(\mathbf{U}^2 - \mathbf{I})\hat{\mathbf{n}} = 0;$$

$$\mathrm{tr}(\mathbf{U})^2 - \det\mathbf{U}^2 - \frac{|\mathbf{a}|^2|\hat{\mathbf{n}}|^2}{4} - 2 \geqslant 0.$$

The proof of this theorem and its physical interpretation are given in Ref. [17]. For our purposes, we note that the cofactor conditions allow for an increased number of lattice deformations that satisfy Eq. (13) without elastic energy.

Materials satisfying the cofactor conditions not only form austenite/martensite microstructures with vanishingly small elastic energy, but also do so for numerous values of the volume fraction f in the range $0 \leqslant f \leqslant 1$. For example, the magnetic alloy $Ni_{45}Co_5Mn_{40}Sn_{10}$ satisfies the cofactor conditions with the following $\mathbf{U}$ [9]:

$$\begin{bmatrix} 1.0054 & 0.0082 & 0 \\ 0.0082 & 1.0590 & 0 \\ 0 & 0 & 0.9425 \end{bmatrix}. \tag{A10}$$

Using variants $\mathbf{U}_1, \mathbf{U}_2$ (and their twin solutions $\mathbf{a}, \hat{\mathbf{n}}$) of $Ni_{45}Co_5Mn_{40}Sn_{10}$, we solve for the three cofactor conditions in the geometrically exact theory:

$$\lambda_2 = 1.00417 \approx 1, \tag{A11}$$

$$\mathbf{a}\cdot\mathbf{U}\,\mathrm{cof}(\mathbf{U}^2 - \mathbf{I})\hat{\mathbf{n}} = 2\times10^{-9} \approx 0, \tag{A12}$$

TABLE X. Stretch tensors for an alloy undergoing cubic-to-monoclinic-II transformation.

Stretch tensor	
$\mathbf{U}_1 = \begin{bmatrix} \alpha & \delta & 0 \\ \delta & \beta & 0 \\ 0 & 0 & \gamma \end{bmatrix}$	$\mathbf{U}_2 = \begin{bmatrix} \alpha & -\delta & 0 \\ -\delta & \beta & 0 \\ 0 & 0 & \gamma \end{bmatrix}$
$\mathbf{U}_3 = \begin{bmatrix} \beta & \delta & 0 \\ \delta & \alpha & 0 \\ 0 & 0 & \gamma \end{bmatrix}$	$\mathbf{U}_4 = \begin{bmatrix} \beta & -\delta & 0 \\ -\delta & \alpha & 0 \\ 0 & 0 & \gamma \end{bmatrix}$
$\mathbf{U}_5 = \begin{bmatrix} \alpha & 0 & \delta \\ 0 & \gamma & 0 \\ \delta & 0 & \beta \end{bmatrix}$	$\mathbf{U}_6 = \begin{bmatrix} \alpha & 0 & -\delta \\ 0 & \gamma & 0 \\ -\delta & 0 & \beta \end{bmatrix}$
$\mathbf{U}_7 = \begin{bmatrix} \beta & 0 & \delta \\ 0 & \gamma & 0 \\ \delta & 0 & \alpha \end{bmatrix}$	$\mathbf{U}_8 = \begin{bmatrix} \beta & 0 & -\delta \\ 0 & \gamma & 0 \\ -\delta & 0 & \alpha \end{bmatrix}$
$\mathbf{U}_9 = \begin{bmatrix} \gamma & 0 & 0 \\ 0 & \beta & \delta \\ 0 & \delta & \alpha \end{bmatrix}$	$\mathbf{U}_{10} = \begin{bmatrix} \gamma & 0 & 0 \\ 0 & \beta & -\delta \\ 0 & -\delta & \alpha \end{bmatrix}$
$\mathbf{U}_{11} = \begin{bmatrix} \gamma & 0 & 0 \\ 0 & \alpha & \delta \\ 0 & \delta & \beta \end{bmatrix}$	$\mathbf{U}_{12} = \begin{bmatrix} \gamma & 0 & 0 \\ 0 & \alpha & -\delta \\ 0 & -\delta & \beta \end{bmatrix}$

$$\mathrm{tr}\mathbf{U}^2 - \det\mathbf{U}^2 - \frac{|\mathbf{a}|^2|\hat{\mathbf{n}}|^2}{4} - 2 = 0.0133 \geqslant 0. \tag{A13}$$

Consequently, $Ni_{45}Co_5Mn_{40}Sn_{10}$ not only satisfies the geometrically exact compatibility condition in Eqs. (12a)–(12c), but has infinite solutions to Eqs. (12a)–(12c) for all values of the volume fraction f in the range $0 \leqslant f \leqslant 1$. However, not all solutions to Eqs. (12a)–(12c) will generate divergence-free magnetization at the phase boundary. Minimizing this demagnetization energy, in addition to the elastic energy, in Eq. (2) is necessary to identify suitable microstructures in the $Ni_{45}Co_5Mn_{40}Sn_{10}$ magnetic alloy. We next examine whether the cofactor solutions for materials such as $Ni_{45}Co_5Mn_{40}Sn_{10}$ satisfy the divergence-free magnetization at the paramagnetic/ferromagnetic interface.

Let the magnetization in the ferromagnetic phase be $\mathbf{m}$ that is oriented along its easy crystallographic axes. In $Ni_{45}Co_5Mn_{40}Sn_{10}$ the magnetization $\mathbf{m}$ in the ferromagnetic (cubic crystal symmetry) phase is along its easy crystallographic axes $\langle 111\rangle = \{[111], [1\bar{1}1], [11\bar{1}], \ldots, [\bar{1}\bar{1}\bar{1}]\}$. The stretch tensor $\mathbf{U}$ describes the cubic-to-monoclinic-II transformation in $Ni_{45}Co_5Mn_{40}Sn_{10}$; see Table X for the general form of this stretch tensor $\mathbf{U}$.

Paramagnetic/ferromagnetic microstructures that have divergence-free magnetization at their interfaces form during phase transformations for

$$\mathbf{m}\cdot\mathbf{K}_1 = 0. \tag{A14}$$

Here, $\mathbf{K}_1$ is the direction of the habit plane separating the paramagnetic and ferromagnetic phases and is obtained by solving the crystallographic theory in Eqs. (12a)–(12c):

$$\mathbf{K}_1 = \frac{\mathbf{U}_J^{-1}\hat{\mathbf{n}}}{|\mathbf{U}_J^{-1}\hat{\mathbf{n}}|}. \tag{A15}$$

Here, $\mathbf{U}_J$ and $\hat{\mathbf{n}}$ are the stretch tensor for the austenite variant and the vector describing the habit plane, respectively. For $Ni_{45}Co_5Mn_{40}Sn_{10}$, we determine the orientation of the habit plane $\mathbf{K}_1$ by computing Eq. (A15) for volume fractions in the range $0 \leqslant f \leqslant 1$. We then compute the condition in Eq. (A14) for each direction of the magnetization (i.e., $\langle 111 \rangle$).

Figure 7 illustrates the condition $\mathbf{m} \cdot \mathbf{K}_1$ and shows that although $Ni_{45}Co_5Mn_{40}Sn_{10}$ satisfies the mechanical compatibility conditions, it satisfies the divergence-free conditions for specific values of the volume fraction. We illustrate these divergence-free microstructures in Fig. 6 using $f = 0$, $f = 1$, and $f = 3/7$ as representative examples.

[1] O. Gutfleisch, M. A. Willard, E. Brück, C. H. Chen, S. G. Sankar, and J. P. Liu, Magnetic materials and devices for the 21st century: Stronger, lighter, and more energy efficient, Adv. Mater. (Weinheim) **23**, 821 (2011).

[2] A. Kitanovski, Energy applications of magnetocaloric materials, Adv. Energy Mater. **10**, 1903741 (2020).

[3] F. Scheibel, T. Gottschall, A. Taubel, M. Fries, K. P. Skokov, A. Terwey, W. Keune, K. Ollefs, H. Wende, M. Farle, M. Acet, O. Gutfleisch, and M. E. Gruner, Hysteresis design of magnetocaloric materials—From basic mechanisms to applications, Energy Technol. **6**, 1397 (2018).

[4] H. Knüpfer, R. V. Kohn, and F. Otto, Nucleation barriers for the cubic-to-tetragonal phase transformation, Commun. Pure Appl. Math. **66**, 867 (2013).

[5] Z. Zhang, R. D. James, and S. Müller, Energy barriers and hysteresis in martensitic phase transformations, Acta Mater. **57**, 4332 (2009).

[6] C. Chluba, W. Ge, R. L. de Miranda, J. Strobel, L. Kienle, E. Quandt, and M. Wuttig, Ultralow-fatigue shape memory alloy films, Science **348**, 1004 (2015).

[7] Please see the Appendix for further details.

[8] The atomically engineered Ti-Ni-Cu shape memory not only showed negligible fatigue after 10^7 cycles,but also did so despite its large transformation strain (∼8%) and despite being subjected to a load of over 300 MPa [6].

[9] Y. Song, X. Chen, V. Dabade, T. W. Shield, and R. D. James, Enhanced reversibility and unusual microstructure of a phase-transforming material, Nature (London) **502**, 85 (2013).

[10] Y. G. Liang, S. Lee, H. S. Yu, H. R. Zhang, Y. J. Liang, P. Y. Zavalij, X. Chen, R. D. James, L. A. Bendersky, A. V. Davydov, X. H. Zhang and I. Takeuchi, Tuning the hysteresis of a metal-insulator transition via lattice compatibility, Nat. Commun. **11**, 3539 (2020).

[11] K. K. Dubey, P. Devi, A. K. Singh, and S. Singh, Improved crystallographic compatibility and magnetocaloric reversibility in Pt substituted $Ni_2Mn_{1.4}In_{0.6}$ magnetic shape memory Heusler alloy, J. Magn. Magn. Mater. **507**, 166818 (2020).

[12] V. Srivastava, Y. Song, K. Bhatti, and R. D. James, The direct conversion of heat to electricity using multiferroic alloys, Adv. Energy Mater. **1**, 97 (2011).

[13] A. R. Balakrishna, J. E. Huber, and I. Münch, Nanoscale periodic domain patterns in tetragonal ferroelectrics: A phase-field study, Phys. Rev. B **93**, 174120 (2016).

[14] I. Muench, A. R. Balakrishna, and J. E. Huber, Periodic boundary conditions for the simulation of 3D domain patterns in tetragonal ferroelectric material, Arch. Appl. Mech. **89**, 955 (2019).

[15] A. Renuka Balakrishna, Crystallographic design of intercalation materials, J. Electrochem. En. Conv. Stor. 1 (2022).

[16] D. Zhang and A. R. Balakrishna, Designing shape-memory-like microstructures in intercalation materials, arXiv:2206.14948 (2022).

[17] X. Chen, V. Srivastava, V. Dabade, and R. D. James, Study of the cofactor conditions: conditions of supercompatibility between phases, J. Mech. Phys. Solids **61**, 2566 (2013).

[18] R. D. James and M. Wuttig, Magnetostriction of martensite, Philos. Mag. A **77**, 1273 (1998).

[19] R. M. Bozorth, *Ferromagnetism* (IEEE, Piscataway, NJ, 1993).

[20] W. F. Brown, *Magnetoelastic Interactions*, Springer-Tracts in Natural Philosophy Vol. 9 (Springer, New York, 1966).

[21] In another line of research, we showed that the fundamental magnetic material constants play a crucial role in governing magnetization reversal under an applied magnetic field and that for a specific combination of these constants, $\frac{(c_{11}-c_{12})\lambda_{100}^2}{2\kappa_1} = 81$, magnetic coercivity can be made to be very small [23–25].

[22] The direction of magnetization $\mathbf{m}$ is in turn determined by the anisotropy constants κ_1, κ_2 of the material.

[23] A. R. Balakrishna and R. D. James, A tool to predict coercivity in magnetic materials, Acta Mater. **208**, 116697 (2021).

[24] A. R. Balakrishna and R. D. James, A solution to the permalloy problem–A micromagnetic analysis with magnetostriction, Appl. Phys. Lett. **118**, 212404 (2021).

[25] A. R. Balakrishna and R. D. James, Design of soft magnetic materials, npj Comput. Mater. **8**, 4 (2022).

[26] J. M. Ball and R. D. James, Fine phase mixtures as minimizers of energy, Arch. Ration. Mech. Anal. **100**, 13 (1987).

[27] E. B. Tadmor, R. E. Miller, and R. S. Elliott, *Continuum Mechanics and Thermodynamics: From Fundamental Concepts to Governing Equations* (Cambridge University Press, Cambridge, 2012).

[28] In the classical continuum framework, magnetization is a volume average of the dipole field over a volume that is larger than individual lattice spacing. Following Ref. [29], we adapt this treatment and identify magnetization as a macroscopic quantity for a family of scaled lattices $L_\gamma := L(\gamma \mathbf{e}_i)$, in which $\mathbf{e}_i$ is a fixed set of orthonormal lattice vectors.

[29] R. D. James and D. Kinderlehrer, Theory of magnetostriction with applications to $Tb_xDy_{1-x}Fe_2$, Philos. Mag. B **68**, 237 (1993).

[30] J. L. Ericksen, On the Cauchy-Born rule, Math. Mech. Solids **13**, 199 (2008).

[31] K. Bhattacharya, *Microstructure of Martensite: Why It Forms and How It Gives Rise to the Shape-Memory Effect*, Oxford Series on Materials Modelling Vol. 2 (Oxford University Press, Oxford, 2003).

[32] P. F. Ladwig, Y. A. Chang, E. S. Linville, A. Morrone, J. Gao, B. B. Pant, A. E. Schlutz, and S. Mao, Paramagnetic to antiferromagnetic phase transformation in sputter deposited Pt–Mn thin films, J. Appl. Phys. (Melville, NY) **94**, 979 (2003).

[33] S. Cui, J. Wan, N. Chen, and Y. Rong, Phase-field simulation of magnetic field induced microstructure evolution in γMn-based alloys, J. Appl. Phys. (Melville, NY) **127**, 095103 (2020).

[34] V. A. L'vov and A. Kosogor, Inverse magnetocaloric effect in the solids undergoing ferromagnetic–antiferromagnetic phase transition: Landau theory applied to Fe-Rh alloys, J. Magn. Magn. Mater. **517**, 167269 (2021).

[35] R. Becker and W. Döring, *Ferromagnetismus* (Springer-Verlag, Berlin, 2013).

[36] Z. H. Liu, M. Zhang, W. Q. Wang, W. H. Wang, J. L. Chen, G. H. Wu, F. B. Meng, H. Y. Liu, B. D. Liu, J. P. Qu, and Y. X. Li, Magnetic properties and martensitic transformation in quaternary Heusler alloy of NiMnFeGa, J. Appl. Phys. (Melville, NY) **92**, 5006 (2002).

[37] Z. Li, J. Yang, D. Li, Z. Li, B. Yang, H. Yan, C. F. Sánchez-Valdés, J. L. S. Llamazares, Y. Zhang, C. Esling, X. Zhao, and L. Zuo, Tuning the reversible magnetocaloric effect in Ni–Mn–In-based alloys through Co and Cu co-doping, Adv. Electron. Mater. **5**, 1800845 (2019).

[38] J. Liu, X. You, B. Huang, I. Batashev, M. Maschek, Y. Gong, X. Miao, F. Xu, N. van Dijk, and E. Brück, Reversible low-field magnetocaloric effect in Ni-Mn-In-based Heusler alloys, Phys. Rev. Materials **3**, 084409 (2019).

[39] Y. Qu, A. Gràcia-Condal, L. Mañosa, A. Planes, D. Cong, Z. Nie, Y. Ren, and Y. Wang, Outstanding caloric performances for energy-efficient multicaloric cooling in a Ni-Mn-based multifunctional alloy, Acta Mater. **177**, 46 (2019).

[40] P. Devi, C. S. Mejía, M. G. Zavareh, K. K. Dubey, P. Kushwaha, Y. Skourski, C. Felser, M. Nicklas, and S. Singh, Improved magnetostructural and magnetocaloric reversibility in magnetic Ni-Mn-In shape-memory Heusler alloy by optimizing the geometric compatibility condition, Phys. Rev. Materials **3**, 062401(R) (2019).

[41] M. Kataoka, K. Endo, N. Kudo, T. Kanomata, H. Nishihara, T. Shishido, R. Y. Umetsu, M. Nagasako, and R. Kainuma, Martensitic transition, ferromagnetic transition, and their interplay in the shape memory alloys $Ni_2Mn_{1-x}Cu_xGa$, Phys. Rev. B **82**, 214423 (2010).

[42] In our calculations, we assume the austenite phase to be nonmagnetic and the martensite (low-symmetry) phase to be magnetic.

[43] The eigenvalues of the strain tensor are ordered such that $\epsilon_1 \leqslant \epsilon_2 \leqslant \epsilon_3$. The eigenvectors correspond to these ordered eigenvalues.

[44] Note that variants $\mathbf{E}_3$, $\mathbf{E}_4$ have the same strain tensor but different magnetizations.

[45] These latter lattice deformations are commonly observed in several magnetocaloric Heusler alloys with easy axes along the $\langle 100\rangle$, $\langle 111\rangle$, and $\langle 110\rangle$ crystallographic directions [9,11,36,37].

[46] When compared with magnetic materials in Sec. III that undergo cubic-to-tetragonal, cubic-to-trigonal, cubic-to-monoclinic-I structural changes.